CHEMISTRY OF MATERIALS

pubs.acs.org/cm

Article

Molecular-Level Characterization of Oxygen Local Environments in a Pristine and Post-Synthetically Modified Metal−Organic Framework via ^{17}O Nuclear Magnetic Resonance Spectroscopy

Vinicius Martins,[#] Bryan E.G. Lucier,[#] Kuizhi Chen, Ivan Hung, Zhehong Gan, Christel Gervais, Christian Bonhomme, Heng-Yong Nie, Wanli Zhang, and Yining Huang*

Cite This: *Chem. Mater.* 2023, 35, 3555−3569

Read Online

ACCESS | Metrics & More | Article Recommendations | Supporting Information

ABSTRACT: Porous metal−organic frameworks (MOFs) have found many technological applications in fields such as carbon capture and storage, catalysis, and selective guest adsorption. Post-synthetic modification (PSM) approaches can influence MOF properties by introducing new functional groups or metals. MIL-121 is a prototypical aluminum MOF containing free uncoordinated carboxylic acid groups, which can act as adsorption sites for metal exchange as they are accessible to guests from within the pores. The introduction of metal species has been proven to enhance the gas adsorption capacity and catalytic properties of MIL-121. A deeper understanding of how MOF carboxylic acid groups interact with metals is imperative for the development of advanced industrially relevant materials. In this work, we demonstrate the remarkable capability of ^{17}O solid-state NMR at 35.2 and 19.6 T to assign each ^{17}O resonance in MIL-121 to its chemical/crystallographic oxygen site, provide site-specific structural information, and probe both the location and binding mode of metal guests within the framework. A series of 1D and 2D ^{17}O NMR experiments on ^{17}O-enriched MIL-121 supported by computational methods have been employed to study changes in the local environments of oxygen upon the activation of the material as well as upon metal loading. These results clearly show that the high spectral resolution achieved via high-field magic-angle spinning (MAS), REDOR (rotational-echo double-resonance), multiple-quantum MAS (MQMAS), and D-HMQC (dipolar heteronuclear multiple-quantum coherence) experiments yields unprecedented insight into this MOF. The ^{17}O NMR parameters provide molecular-level information regarding the local oxygen environment, intermolecular interactions, and host−guest connectivity. This experimental approach can be applied to a wide variety of oxygen-containing MOFs.

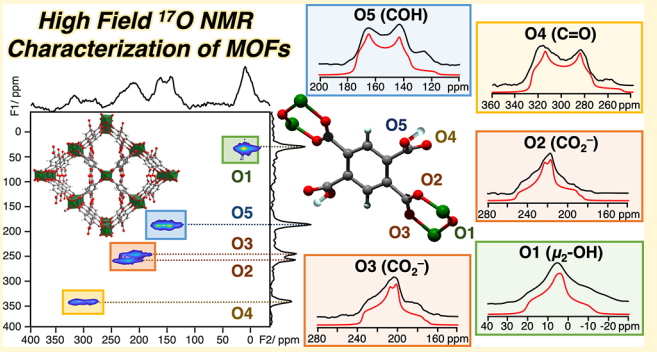

INTRODUCTION

Metal−organic frameworks (MOFs) are a unique class of porous materials synthesized via the combination of organic linkers and inorganic nodes to form three-dimensional frameworks. These materials afford scientists exceptional control over the MOF composition, topology, and resulting physicochemical properties, which can be fine-tuned to address specific applications.[1−3] When desired MOF properties cannot be achieved through a purely synthetic route, post-synthetic modification (PSM) can be used to introduce new functional groups or metals into the framework. PSM can include approaches such as modifying the organic linker and/or metal node as well as the adsorption or exchange of guest species.[4,5] PSM has been widely employed to introduce new features to MOFs, such as enhanced chemical stability, increased gas adsorption capability, and catalytic activity.[4−7] MOFs bearing free carboxylic acid (COOH) groups on the linker are ideal platforms for PSM as the uncoordinated COOH groups can act as reactive anchor sites for introducing additional metal ions or for further PSM.[8,9]

A prototypical aluminum MOF containing uncoordinated COOH groups is MIL-121, which is composed of 1,2,4,5-benzenetetracarboxylate (pyromellitate, BTEC) linkers and aluminum centers assembled into a three-dimensional microporous framework (Figure 1).[10] The structure of MIL-121 involves infinite chains of $AlO_4(OH)_2$ octahedra connected by hydroxyl groups. The chains are then linked to each other by bridging BTEC ligands. Two carboxylate groups of the BTEC ligand are coordinated to the Al^{3+} metal centers, while the two

Received: January 28, 2023
Revised: April 5, 2023
Published: April 20, 2023

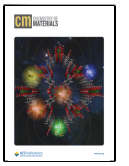

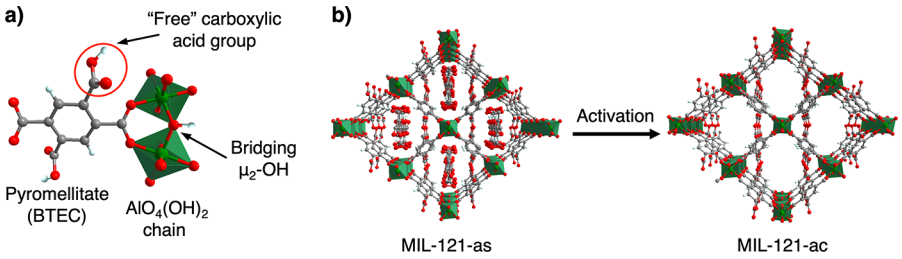

Figure 1. (a) Pyromellitate (BTEC) linker and $AlO_4(OH)_2$ building blocks underpinning the structure of MIL-121; (b) activation process of MIL-121 in which MIL-121-as contains unreacted pyromellitic acid ligands inside the pores, which are then removed by heat and vacuum.

uncoordinated "free" COOH groups are directed toward the pore interior and are accessible to guests. The as-made form contains disordered unreacted BTEC and water guests, which can be removed by solvent exchange followed by activation, preserving the crystalline framework structure and yielding activated MIL-121-ac.[10] The long-range structure of MIL-121 is similar to that of MIL-53 in its large pore configuration;[11,12] however, MIL-53 does not contain uncoordinated COOH groups on the linkers.

The BTEC linker and associated free COOH groups within MIL-121 present extensive controllable PSM opportunities. A hierarchical pore structure can be created in MIL-121 via PSM; pore expansion is first achieved via thermal decarboxylation of the linker then a subsequent additional decarboxylation introduces hierarchical porosity in MIL-121 and increases the surface area, enhancing the gas adsorption uptake for industrially relevant gases such as CO_2, C_2H_2, C_2H_4, and CH_4.[13] The pores of MIL-121 can be decorated with highly reactive anhydride groups via thermolysis, which enables the binding of several guest molecule classes including alcohols, amines, thiols, and noble metal complexes.[8] The free COOH groups in MIL-121 serve as the active sites for interaction with guest species and can be used to introduce non-framework metal ions.[14−17] The PSM of MIL-121 to add Li^+, Mg^{2+}, and Ca^{2+} results in materials with an enhanced uptake of H_2 and CO_2,[17] and Li-loaded MIL-121 has shown promise as an electrolyte for solid-state batteries.[15]

The MIL-121 MOF and its derivative materials obtainable through PSM highlight the fundamental role that COOH groups play in the synthesis, structure, and potential applications of MOFs.[18] A comprehensive molecular-level understanding of interactions between COOH, guests, and metals is imperative to drive MOFs further toward industrially relevant applications. MOFs are typically characterized via single-crystal or powder X-ray diffraction (XRD), which yields atomic positions and unit cell parameters. X-ray-based techniques cannot provide complete information on the fine local structure around the framework species and the local environment around disordered guests, and they do not identify hydrogen positions and offer limited information on hydrogen-bonding interactions within MOFs; all of which are critical when COOH groups are involved.

Solid-state NMR (SSNMR) spectroscopy is a site-specific characterization technique that yields information on short and long-range structure in MOFs[19−21] and is an excellent complement to XRD-based methods. Prior ^1H and ^{13}C NMR experiments on various forms of MIL-121 have shown that an NMR-based approach can yield a wealth of local information in this particular system,[17] but there are limitations to such an approach. While ^1H NMR is a natural choice for investigating COOH groups and their associated chemistry in MIL-121, the carboxylic hydrogen is often deprotonated via pH control to expose a reactive CO_2^- group, removed during PSM, or lost via reactions with guests, leaving no hydrogen proximate to the site of interest. In contrast, the oxygen atoms within COOH groups are far less frequently removed and are intimately involved in host−guest interactions. In addition to being within the free COOH groups, MIL-121 also features oxygen within the carboxylate group (CO_2^-) coordinated to Al and the hydroxyl group (μ_2-OH) bridging two AlO_6 octahedra (Figure 1). ^{17}O is an NMR-active nucleus with a reasonably large chemical shift range that provides data on the local electronic and magnetic environments in systems containing organic components,[22] including microporous materials such as MOFs.[23] The ^{17}O nucleus is subject to both the magnetic chemical shift and electric quadrupolar interactions, which offer independent information on the local chemical environment and molecular interactions such as hydrogen bonding and metal−ligand interactions within MOFs.[23−28] We have recently demonstrated that performing NMR experiments at a high magnetic field of 35.2 T unlocks remarkable ^{17}O spectral resolution, such as the identification of all 12 crystallographically inequivalent oxygen sites in a MOF, and shown how ^{17}O NMR is exquisitely sensitive to subtle changes in a local environment during MOF activation.[29] More pronounced changes, such as a MOF phase transition in MIL-53, can also be followed by high-field ^{17}O NMR spectroscopy.[26,30]

In this work, we have acquired ^{17}O NMR spectra of ^{17}O-enriched MIL-121 samples at high magnetic fields of 19.6 and 35.2 T to study the local environments of each distinct oxygen site. Both the as-made and activated MIL-121 phases are investigated, culminating in a structural assignment of ^{17}O resonances to unique sites in the crystal structure, which is aided and verified by ab initio calculations. To demonstrate the feasibility of ^{17}O NMR for the characterization of MOFs after PSM, local oxygen environments were also probed in MIL-121 derivates loaded with non-framework metal ions of various valences, sizes, and polarization ($M = Na^+$, Ca^{2+}, Ag^+, In^{3+}), which yielded sufficient data to draw meaningful conclusions regarding the metal ion location, binding, and local disorder within the MOF when Na^+ and Ag^+ ions were involved.

EXPERIMENTAL SECTION

Materials. All materials were used as purchased from commercial suppliers without further purification. The silver acetate reagent and the silver-exchanged Ag@MIL-121 MOF were handled in a dark room to avoid the oxidation of the silver cations.

Synthesis of ^{17}O-Enriched MIL-121. The main impediment to ^{17}O enrichment of MOFs is the significant financial cost of isotopically labeled reagents.[25,31] We based our approach on a reported method requiring 20.0 mL of deionized H_2O and 3.2 mL of 4.0 M HNO_3. Given the cost of ^{17}O-enriched water, routes involving

https://doi.org/10.1021/acs.chemmater.3c00199
Chem. Mater. 2023, 35, 3555−3569

smaller volumes of water were explored. Scaling volumes down by half reduced the required deionized water volume to 10.0 mL along with 1.6 mL of 4.0 M HNO_3.[17] We attempted to optimize this synthesis using water volumes of 10.0, 8.0, 6.0, and 4.0 mL with powder X-ray diffraction used to verify the MOF structure (Figure S1). The volume of 4.0 M HNO_3 was scaled in line with the water volume in order to maintain the reported[17] 10:1.6 v/v ratio of H_2O:HNO_3. We found 4.0 mL of water in total to be the optimal value; in our syntheses of ^{17}O-enriched MIL-121 samples, 3.5 mL of deionized water and 0.5 mL of 35 atom % $H_2{}^{17}O$ (l) were used along with 0.64 mL of 4.0 M HNO_3. After establishing the appropriate amount of water required, the synthesis of MIL-121 was then performed. Into a solid mixture of 4.80 g of $Al(NO_3)_3{\cdot}9H_2O$ (Alfa Aesar, 98%) and 1.20 g of 1,2,4,5-benzenetetracarboxylic acid (Sigma-Aldrich, 96%), 3.5 mL of deionized water and 0.5 mL of ^{17}O-enriched H_2O (CortecNet, 35 atom %) were added along with 0.64 mL of 4.0 HNO_3 (diluted from Sigma-Aldrich concentrated HNO_3) within a 23.0 mL Teflon-lined stainless-steel autoclave. The mixture was sonicated for 8 min; following which, the autoclave was sealed and heated at 90 °C for 24 h. The as-made MIL-121 (MIL-121-as) product was collected as a white powder, which was isolated by centrifugation and dried in an oven at 90 °C overnight.

Solvent Exchange and Activation. An amount of 0.20 g of MIL-121-as was dispersed in 20.0 mL of methanol (MeOH) and heated in a sealed Teflon-lined stainless-steel autoclave at 150 °C for three days. During this time, the MeOH was decanted and replaced with fresh MeOH every 24 h. The solvent-exchanged MIL-121 product was collected by centrifugation and dried overnight at 80 °C. Finally, solvent-exchanged MIL-121 was heated at 250 °C under a dynamic vacuum for 24 h to yield activated MIL-121, which is termed as MIL-121-ac.

Ion Exchange Experiments. The metal-loading procedure was carried out following the procedure from a previous work in order to introduce the maximum possible amount of each specific metal ion within MIL-121.[17] This procedure involves using experimental conditions such as the ion reagent concentration, replacement of ion reagents, reaction time, and reaction conditions that are specific to each guest ion being introduced.

Na@MIL-121: 0.10 g of MIL-121-ac was stirred in 10.0 mL of 0.2 M Na_2CO_3 for 15 min at room temperature; after which the solid was isolated via centrifugation, washed with deionized water, and then dried at 80 °C overnight.

Ca@MIL-121: 0.10 g of MIL-121-ac was mixed with 10.0 mL of a $Ca(OH)_2$ saturated solution for 15 min at room temperature. The solid was decanted off via centrifugation, and the solution was then replaced with a fresh 10.0 mL $Ca(OH)_2$ saturated solution and stirred for another 10 min. At the end, the sample was collected by centrifugation and dried at 80 °C overnight.

Ag@MIL-121: 0.10 g of MIL-121-ac was introduced to 5.0 mL of 0.08 M $Ag(CH_3CO_2)$ and then stirred for ca. 15 h at 90 °C in an oil bath. The final product was then isolated from the mixture via centrifugation, washed with deionized water, and dried at 80 °C overnight.

In@MIL-121: 0.10 g of MIL-121-ac was mixed with 10.0 mL of 0.0015 M $In(CH_3CO_2)_3$ and stirred for three days. The $In(CH_3CO_2)_3$ solution was decanted off and replaced daily for a total of three times. The solid was then collected by centrifugation, washed with deionized water, and dried at 80 °C overnight.

Time-of-Flight Secondary Ion Mass Spectrometry (TOF-SIMS). TOF-SIMS experiments were carried out to estimate ^{17}O enrichment in MOF samples.[25] The samples were pressed between two silicon wafers coated with an indium layer and then were separated to obtain a cross section of the pressed particles. Experiments were performed at the Surface Science Western facility located at the University of Western Ontario using an ION-TOF (Gmbh) TOF-SIMS IV instrument equipped with a Bi cluster liquid metal ion source that was used to estimate the ratio of ^{17}O to ^{16}O. A 25 keV Bi_3^+ cluster primary pulsed ion beam (pulse width < 2 ns, target current ~1 pA) was employed to bombard the surface of the sample in order to generate secondary ions. The secondary ions were extracted from the sample surface and separated by their masses with their arrival times detected via a reflection time-of-flight analyzer. The arrival times were converted to mass-to-charge ratios (m/z) using H^-, C^-, and C_4H^- as well as other known species if needed. Negative secondary ion mass spectra were collected for 120 s at 128 × 128 pixels by rastering the Bi_3^+ ion beam over an area of 500 μm × 500 μm at three spots on each sample.

To estimate the ^{17}O enrichment level, the relative intensities of the peaks associated with $^{16}O_2^-$ at m/z 32 and $^{17}O_2^-$ at m/z 34 were analyzed in triplicate. First, the average of the $^{16}O_2^-/^{17}O_2^-$ ratios was taken. A value of 0.401% was then subtracted from the averaged values to account for the contribution from the $^{16}O^{18}O^-$ isotopomer at m/z 34 overlapping with the signal from the $^{17}O_2^-$ isotopomer. Assuming $^{17}O_2^-/^{16}O_2^- = {}^{17}O/{}^{16}O$, the $^{17}O/^{16}O$ isotope ratios were then determined. The ^{17}O isotopic enrichment levels are listed in Table S1. The $^{17}O/^{16}O$ percentage ratios estimated for the MIL-121 samples are as follows: MIL-121-as, 4.24 ± 0.12%; MIL-121-ac, 5.51 ± 0.11%; Na@MIL-121, 2.67 ± 0.06%; Ca@MIL-121, 3.95 ± 0.06%; Ag@MIL-121, 4.37 ± 0.24%; and In@MIL-121 4.39 ± 0.13%.

Powder X-ray Diffraction (PXRD). Experiments were performed on an Inel CPS powder diffractometer equipped with an Inel CPS 120 detector operating at 40 kV and 40 mA using Cu Kα radiation (λ = l.5418 Å). The diffraction data was collected at 2θ angles ranging from 5 to 120° to confirm the identity, crystallinity, and phase purity of MIL-121 along with its metal-exchanged derivatives. Experimental diffractograms of both the as-made and activated samples matched well with the simulated diffractogram generated from the reported single-crystal structure of MIL-121-as (CCDC: 883608).[10] The metal exchanged-MIL-121 diffractograms (Figure S2) agree with a previous report[17] and confirm that the framework integrity was preserved after metal loading.

Inductively Coupled Plasma Mass Spectrometry (ICP-MS). The metal exchange level in MIL-121 samples was determined using an Agilent 7700 ICP-MS spectrometer at the Biotron Research Centre at Western University. The reference method used was EPA 200.8.[32]

Thermogravimetric Analyses (TGA). Experiments were carried out on a Mettler Toledo TGA/SDTA851e instrument from 30 to 900 °C under a N_2 flow using a heating rate of 10 °C min^{-1}. The TGA curve of MIL-121-as (Figure S3) features a weight loss in two stages until framework decomposition at ca. 400 °C, which correspond to a loss of solvent and unreacted ligands from the pores. The TGA curve of methanol-exchanged MIL-121 displays a relatively smaller weight loss up to ca. 400 °C due to the guest methanol leaving the pores, following which the framework decomposes. The thermogram of MIL-121-ac does not show any weight loss until framework decomposition at ca. 350−400 °C, which confirms that all pores are largely free of guests.

Solid-State NMR Measurements. SSNMR spectra at 35.2 T ($\nu_0(^{17}O)$ = 203.4 MHz) were acquired at the National High Magnetic Field Laboratory (NHMFL) in Tallahassee, Florida, USA using the series-connected hybrid (SCH) magnet,[33] a Bruker Avance NEO spectrometer, a custom-made 3.2 mm low-γ MAS probe, and a spinning rate of 18 kHz. SSNMR data at 19.6 T ($\nu_0(^{17}O)$ = 112.7 MHz) were obtained at the NHMFL using a Bruker Avance NEO spectrometer, a 3.2 mm HX MAS probe, and a spinning frequency of 16 kHz. All ^{17}O NMR spectra were referenced to water at 0 ppm.[34] Additional details are provided in Tables S2−S7.

^{17}O one-dimensional (1D) MAS spectra were acquired using a 1D rotor-synchronized spin-echo pulse sequence. $^{17}O\{^1H\}$ rotational-echo double-resonance (REDOR)[35,36] spectra were acquired with ^{17}O and ^1H rf fields of 27.8 and 50 kHz, respectively. $^{17}O\{^1H\}$ correlation spectra were acquired with the dipolar heteronuclear multiple-quantum correlation (D-HMQC) experiment[37,38] using the $SR4^2_1$ sequence[39] on the indirect ^1H channel for dipolar recoupling with an rf field equal to twice the spinning frequency (i.e., 32 kHz). ^{17}O two-dimensional (2D) triple-quantum MAS (3QMAS) NMR spectra were acquired using a rotor-synchronized shifted-echo 3QMAS pulse sequence to avoid spinning sidebands along the indirect F1 dimension,[40] which are due to 3Q excitation/conversion modulation

https://doi.org/10.1021/acs.chemmater.3c00199
Chem. Mater. 2023, 35, 3555−3569

and/or the significant ^{17}O chemical shift anisotropy (CSA) observed at very high fields. All F1 spinning sidebands are folded back onto the central band, enhancing the overall sensitivity of MQMAS experiments, especially for sites associated with large quadrupole coupling constants and CSA.[40−42] The Q-shearing processing method[43] was used to unfold spinning sidebands and peaks aliased into the F1 spectral window equal to the spinning frequency. The 3Q excitation and conversion pulses were 3.0 and 1.0 μs, respectively.

Spectral Simulations. The Dmfit software package was used to simulate SSNMR spectra using the Int2QUAD mode, which incorporates both quadrupolar and CSA effects.[44]

NMR Interactions and Tensor Conventions. The ^{17}O isotope has a spin of 5/2 and is subject to two significant interactions that broaden lines and impart characteristic lineshapes in ^{17}O NMR spectra: the second-order electric quadrupolar interaction owing to the quadrupolar moment of ^{17}O[45] and the chemical shift (CS) interaction. The reader is directed toward Appendix A in the Supporting Information for a brief description of these interactions and conventions.

Theoretical Calculations. The unit cell parameters and atomic positions were set to values from the reported MIL-121 crystal structure.[10] Missing hydrogen atoms were initially positioned to be consistent with the expected structure of the system, and all atomic positions were then optimized using the VASP (Vienna ab initio simulation package) code[46] based on the Kohn−Sham density functional theory (DFT) and using a plane-wave pseudopotential approach. The NMR parameters were calculated within the Kohn−Sham DFT using the QUANTUM-ESPRESSO code.[47] The Perdew−Burke−Ernzerhof (PBE) generalized gradient approximation[48] was used, and the valence electrons were described by norm-conserving pseudopotentials[49] in the Kleinman−Bylander form.[50] The wave functions were expanded on a plane wave basis set with a kinetic energy cutoff of 80 Ry. The integral over the first Brillouin zone was performed using a Monkhorst−Pack 1 × 1 × 3 (activated structure) or 1 × 1 × 1 (double-cell as-made structure) k-point grids for the charge density and magnetic shielding tensor calculation. The electric field gradient (EFG) and magnetic shielding tensors were computed using the gauge-including projector augmented wave (GIPAW) approach.[51−53] The isotropic chemical shift, δ_{iso}, is defined as $\delta_{iso} = \sigma_{iso} - \sigma_{iso}(ref)$, where σ_{iso} is the isotropic magnetic shielding and $\sigma_{iso}(ref)$ is the isotropic magnetic shielding of the same nucleus in a reference compound. In this case, the fit of the linear correlation between the experimental δ_{iso} and the calculated σ_{iso} values of ^{17}O for Na_2SiO_3, α-$Na_2Si_2O_5$, α- and γ-glycine, and α-$SrSiO_3$ enabled the determination of the relation between δ_{iso} and calculated σ_{iso} for the ^{17}O nucleus, as described previously.[54]

RESULTS AND DISCUSSION

^{17}O MAS NMR Experiments at 19.6 T. A fundamental understanding of the crystal structure of MIL-121 and its oxygen sites is necessary to interpret ^{17}O NMR spectra. MIL-121-as contains 13 crystallographically unique oxygen atoms (Figure 2) that can be classified into several groups. There are two oxygens from the carboxylate moiety coordinated to Al^{3+} cations (O2 and O3, CO_2^- group), one oxygen atom in the hydroxyl position (O1, 1/2 occupancy, μ_2-OH group), two oxygens from the "free" uncoordinated carboxylic acid linker groups (O4 of the C═O portion and O5 of COH), and eight disordered oxygen atoms originating from uncoordinated BTEC ligands occupying the pores (O21−O28).[10] The crystal structure of MIL-121-ac has not been reported; however, PXRD suggests that the structure of the activated phase remains the same as that of the as-made phase upon removal of the uncoordinated organic ligand and water from the pores (Figure S2).[10] This assumption means that the crystal structure of MIL-121-ac contains five unique oxygen sites

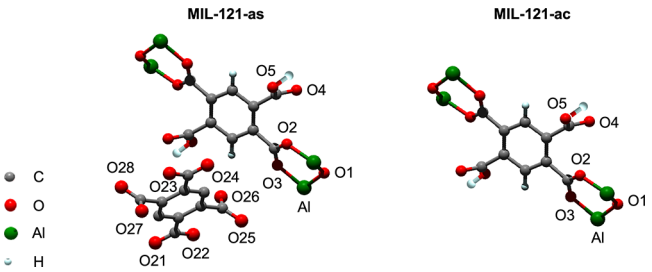

Figure 2. The five crystallographically unique oxygen sites in the MIL-121-as and MIL-121-ac MOFs are shown, labeled O1−O5. The additional eight unique oxygen sites on the uncoordinated BTEC ligands within the pores of MIL-121-as are numbered O21−O28. Note that the unit cells of MIL-121-as and MIL-121-ac are comparable but not exactly the same.

numbered in the same fashion as the framework sites within MIL-121-as.

The ^{17}O isotope has a rather large NMR chemical shift range,[55] and using similar systems as a model, we can understand where ^{17}O resonances from the five unique sites in MIL-121-as and -ac should be found. In general, the C═O oxygen of a carboxylic acid resonates from 260 to 340 ppm, while COH oxygen signals lie between 120 and 200 ppm. In the case of hydrogen bonding, both COH and C═O exhibit chemical shifts ranging from 220 to 300 ppm.[55] Phthalic acid is a good reference because of its similarity to the BTEC linker in MIL-121. The ^{17}O MAS NMR spectrum of phthalic acid comprises two resonances at 312 and 180 ppm, which have been assigned to the carboxylic acid C═O and COH oxygen sites, respectively.[56,57] The topology of the large-pore MIL-53 MOF phase is similar to that of MIL-121 and provides another useful reference point. The ^{17}O chemical shift of the MIL-53(Al) framework CO_2^- carboxylate group coordinated to the Al^{3+} centers is 236 ppm, and that of the μ_2-OH bridging hydroxyl group is 27 ppm.[29]

The ^{17}O 1D MAS SSNMR spectra of MIL-121-as and MIL-121-ac at 19.6 T and 35.2 T are depicted in Figure 3. The 19.6 T spectrum features four distinct signals at chemical shifts of ca. 20, 175, 240, and 330 ppm along with multiple spinning sidebands produced by the MAS technique that do not

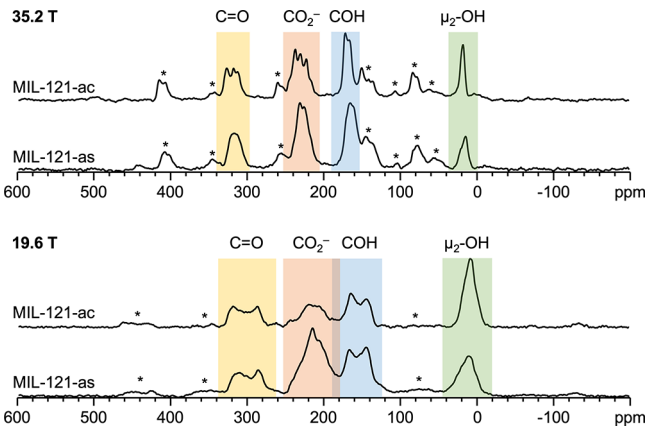

Figure 3. ^{17}O 1D MAS SSNMR spectra of MIL-121-as and MIL-121-ac acquired at 35.2 and 19.6 T with spinning rates of 18 and 16 kHz, respectively. An asterisk (*) denotes positions of the MAS spinning sidebands, which, in some cases, overlap with the isotropic shift signals; see text and Figure 8.

https://doi.org/10.1021/acs.chemmater.3c00199
Chem. Mater. 2023, 35, 3555−3569

represent unique signals. Performing ^{17}O SSNMR measurements at the highest accessible magnetic field strength can enhance the spectral resolution and the accuracy of ^{17}O NMR parameters. The signals in the 1D MAS spectra at 35.2 T are considerably narrower and exhibit well-defined features versus those at 19.6 T. The observed ^{17}O resonance positions and lineshape features in these 1D MAS spectra have contributions from the ^{17}O chemical shift and quadrupolar interactions. These interactions are field-dependent, which leads to slightly different observed resonance positions and lineshapes at 19.6 and 35.2 T. For example, the ^{17}O spinning sidebands are significantly enhanced at higher fields because the CS interaction scales proportionately with the magnetic field. The enhanced CS interaction at 35.2 T is advantageous as the intense and well-resolved spinning sidebands permit more reliable simulations that better quantify the CS NMR parameters. The quadrupolar interaction scales inversely proportionately with the magnetic field and thus has a significantly smaller broadening influence at 35.2 T, which should enhance the spectral resolution. Unfortunately, even at 35.2 T, the overlapping O2 and O3 signals of CO_2^- groups cannot be fully resolved, and only four distinct signals are observed.

A finding of four signals is inconsistent with the five unique oxygen sites in the MIL-121-as crystal structure, and given the distinct ranges of chemical shifts, the discrepancy likely arises from two overlapping ^{17}O NMR signals corresponding to two oxygen atoms in nearly identical local environments. The most chemically similar oxygen sites are O2 and O3 within the CO_2^- carboxylate groups coordinated to Al^{3+} centers. Based on the MIL-121 crystal structure and the reported ^{17}O chemical shift values in similar environments, the signal at 20 ppm corresponds to O1 of the bridging μ_2-OH group, the resonance at 175 ppm to O5 of −COH in free carboxylic acid groups on the linker, the signal at 240 ppm to O2 and O3 of the carboxylate CO_2^- group coordinated to the Al^{3+} centers, and the resonance at 330 ppm to O4 in C═O of the uncoordinated carboxylic acid linker groups. In MIL-121-as, the signals of the oxygen nuclei residing on unreacted ligands within the MOF pores (O21-O28) overlap with the signals of framework ligands in the C═O and COH regions. The signals of O21−O28 on unreacted ligands have very similar chemical environments to the corresponding incorporated linkers and cannot be resolved even at 35.2 T. The lack of resolved O21−O28 signals can also be attributed to the structural disorder of the unreacted BTEC linker, as indicated from XRD data, which should give rise to relatively broader ^{17}O NMR signals for O21−O28 with a lack of distinct features.

^{17}O{^{1}H} REDOR NMR Experiments. In order to unambiguously assign the ^{17}O NMR resonances in MIL-121, several 1D and 2D ^{17}O NMR experiments were performed. The REDOR[58] pulse sequence utilizes the heteronuclear magnetic dipolar interaction between two nuclei, in this case ^{17}O and ^{1}H, to provide information regarding the internuclear proximity (i.e., the O−H distance). Although not employed in this study, the REAPDOR pulse sequence[59] could alternately be used to investigate the proximity since ^{17}O is a quadrupolar nucleus. The ^{17}O{^{1}H} REDOR spectra of MIL-121-as and MIL-121-ac at 19.6 T with a dephasing time of two rotor revolutions (0.062 ms) are shown in Figure 4. The REDOR difference spectra (ΔS) between the control spin echo spectrum (S_0) and the dipolar dephased spectrum (S) is a measure of the O−H dipolar interaction and contains three

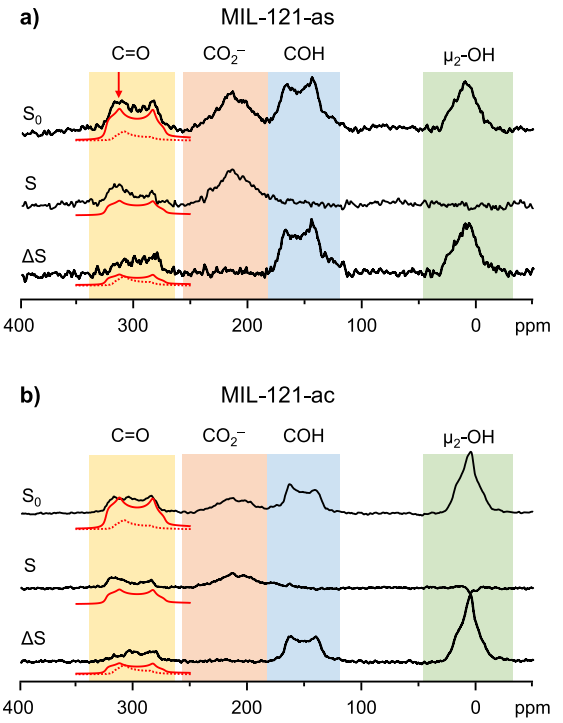

Figure 4. ^{17}O{^{1}H} REDOR spectra of (a) MIL-121-as and (b) MIL-121-ac acquired at 19.6 T and a spinning frequency of 16 kHz. The S_0 spectrum was obtained using a ^{17}O spin-echo experiment, the S spectrum was generated from a REDOR experiment with a dephasing time of 0.062 ms, and the ΔS plot at bottom is the REDOR difference calculated from S_0 − S. The red simulated spectral portions in the C═O region consist of the actual C═O signal (red solid line) along with the COH spinning sideband (red dashed line); see text for details. The signal-to-noise ratio of the MIL-121-as ^{17}O NMR spectrum is relatively lower, owing to a lower wt % of ^{17}O nuclei per unit weight of the MOF sample (i.e., lower density of ^{17}O) arising from the presence of the unreacted ligand within the MOF pores.

signals at 20, 175, and 330 ppm, signifying that the three corresponding types of oxygen environments must be proximate to hydrogen atoms.

Based on the observed REDOR effects, the origins of each ^{17}O signal can be confirmed. The resonance at 20 ppm exhibits a very strong REDOR effect ($\Delta S/S_0$) of almost 100%, indicating that hydrogen is close by, and originates from the bridging μ_2-OH O1 site, which has a directly bound hydrogen. The signal at 175 ppm displays a slightly weaker REDOR effect of 90% and corresponds to the COH O5 site, which also has a directly bound hydrogen. In contrast, the ^{17}O resonance from O4 of C═O groups at 330 ppm yields a REDOR effect of 50%; O4 is not directly attached to a hydrogen atom, and the nearby carboxylic acid hydrogen is relatively longer 1.6 Å away, resulting in a smaller REDOR effect. Of particular note is the lineshape change in the C═O region at 330 ppm between the control and dephased spectra, which introduces a challenge to REDOR analysis. In the control spectrum, the ^{17}O NMR signal intensity at ca. 330 ppm is composed of the actual C═O resonance plus an overlapping spinning sideband from the COH signal (vide infra, Figure 8). In the dephased spectrum, there is no lineshape contribution from the COH oxygen spinning sideband. To accurately calculate the REDOR effect in the difference spectrum, we used only the C═O signal contribution and neglected the spinning sideband artifact from COH. A final observation is the lack of a REDOR effect for the

https://doi.org/10.1021/acs.chemmater.3c00199
Chem. Mater. 2023, 35, 3555−3569

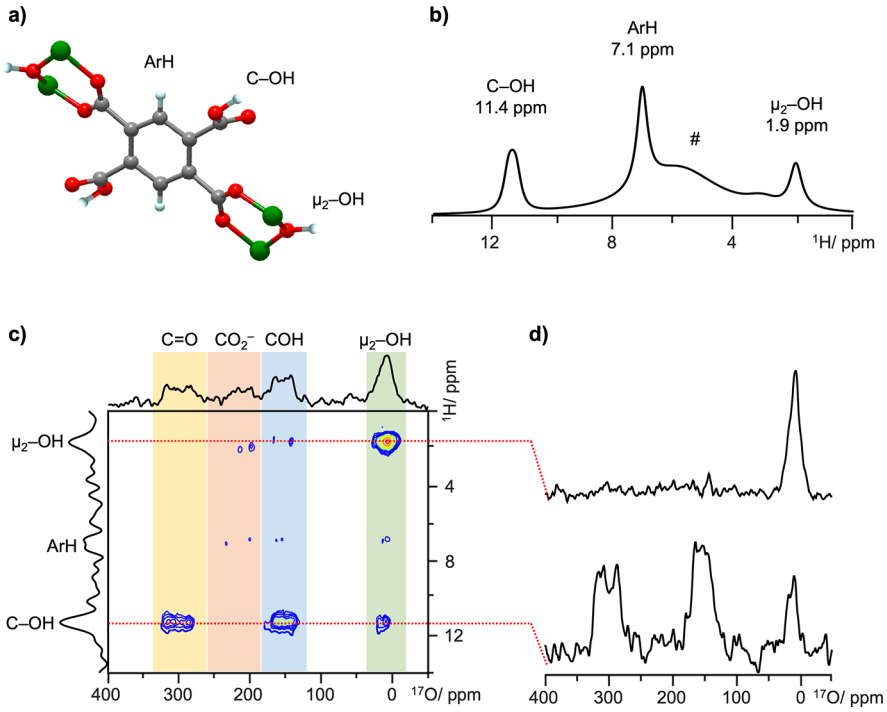

Figure 5. (a) Representation of the different hydrogen species in MIL-121-ac; (b) ^{1}H MAS spectrum of MIL-121-ac at 19.6 T and spinning at 16 kHz; (c) ^{17}O/^{1}H D-HMQC spectrum of MIL-121-ac acquired at 19.6 T with a spinning frequency of 16 kHz; (d) slices of the ^{17}O dimension at the ^{1}H signals. The label # in b denotes the ^{1}H NMR signal originating from adsorbed water inside the pores.

signal at ca. 225 ppm, which agrees with the tentative assignment of O2 and O3 to CO_2^- groups directly bound to Al. There are no hydrogen atoms directly bound or immediately proximate to O2 and O3, which agrees with the absence of a REDOR effect upon this ^{17}O NMR signal. The REDOR results, in conjunction with past reports on similar systems, support our proposed structural assignment of ^{17}O resonances in MIL-121. To confirm this hypothesis and resolve the overlapping O2 and O3 CO_2^- signals, 2D ^{17}O NMR experiments were performed in conjunction with ab initio calculations.

2D ^{17}O NMR Experiments at 19.6 T. The ^{17}O/^{1}H D-HMQC experiment correlates proximate ^{1}H and ^{17}O nuclei via the heteronuclear magnetic dipolar interaction. To establish ^{1}H−^{17}O correlations, all resonances in the ^{1}H MAS spectrum of MIL-121-ac must first be assigned (Figure 5a,b). There are three resonances at ca. 11, 7, and 2 ppm in the ^{1}H NMR spectrum of MIL-121-ac that are assigned to the hydrogen of the free carboxylic acid group on the BTEC linker, the hydrogen on the linker aromatic ring, and the hydrogen of the μ_2-OH bridging hydroxyl groups, respectively.[10,17] The 2 ppm chemical shift of the μ_2-OH bridging hydroxyl group is consistent with the limited hydrogen-bonding network about the OH group in this material; this shift significantly differs from that of the free carboxylic acid hydrogen atoms, which resides in a much more extensive hydrogen-bonding environment. The broad signal at ca. 5 ppm originates from water adsorbed within the MOF; water adsorption from air can occur during packing of the MIL-121 sample into the rotor prior to NMR measurements. TGA data reveals the presence of water in both MIL-121-as and -ac via a gradual weight loss between 0 and ca. 400 °C (Figure S3).

The 2D ^{17}O/^{1}H D-HMQC spectrum of MIL-121-ac (Figure 5c) agrees with our proposed ^{17}O NMR spectral assignments. There is a very strong correlation between the ^{17}O μ_2-OH signal at 22 ppm and the ^{1}H μ_2-OH signal at 1.9 ppm (Figure 5d). The other significant correlations are between the ^{17}O C═O (O4) and COH (O5) signals at 333 and 177 ppm, respectively, with the ^{1}H carboxylic acid signal at 11.4 ppm, confirming that all H and O carboxylic group atoms are in close proximity. The ^{1}H carboxylic acid signal also correlates with the ^{17}O μ_2-OH (O1) signal, which signifies that the hydrogen atom of the free carboxylic acid is spatially proximate to the bridging hydroxyl oxygen. The ^{17}O signal at 240 ppm logically does not correlate with any hydrogen in the framework as both the O2 and O3 oxygen atoms of the CO_2^- group are directly bound to aluminum with no hydrogen atoms nearby.

To continue with ^{17}O spectral assignment, ^{17}O 3QMAS experiments were used to resolve the overlapping O2 and O3 signals from the CO_2^- group. 3QMAS experiments produce a ^{17}O NMR spectrum free of anisotropic quadrupolar interaction influence along the indirect F1 dimension, resulting in significantly narrower signals that should be readily distinguishable.[60,61] The ^{17}O 2D 3QMAS spectra of MIL-121-as and MIL-121-ac at 19.6 T (Figure 6) feature five ^{17}O resonances fully resolved in the F1 dimension and yield their respective quadrupolar parameters via simulations of individual slices in the F2 dimension (Table S8). Both forms of MIL-121 yield distinct ^{17}O 3QMAS signals corresponding to one μ_2-OH, one COH, two CO_2^-, and one C═O environment with chemical shifts listed in Table S8. The observed ^{17}O δ_{iso} values are very similar between each O site in MIL-121-as and -ac, confirming that the local structures about oxygen are nearly identical. In MIL-121-as and -ac, the bridging hydroxyl oxygen O1 is assigned to δ_{iso} = 22 ppm, the free COH species O5 to δ_{iso} = 178 and 177 ppm, and the free C═O species O4 to δ_{iso} = 332 and 334 ppm, respectively. The two overlapping CO_2^- signals

https://doi.org/10.1021/acs.chemmater.3c00199
Chem. Mater. 2023, 35, 3555−3569

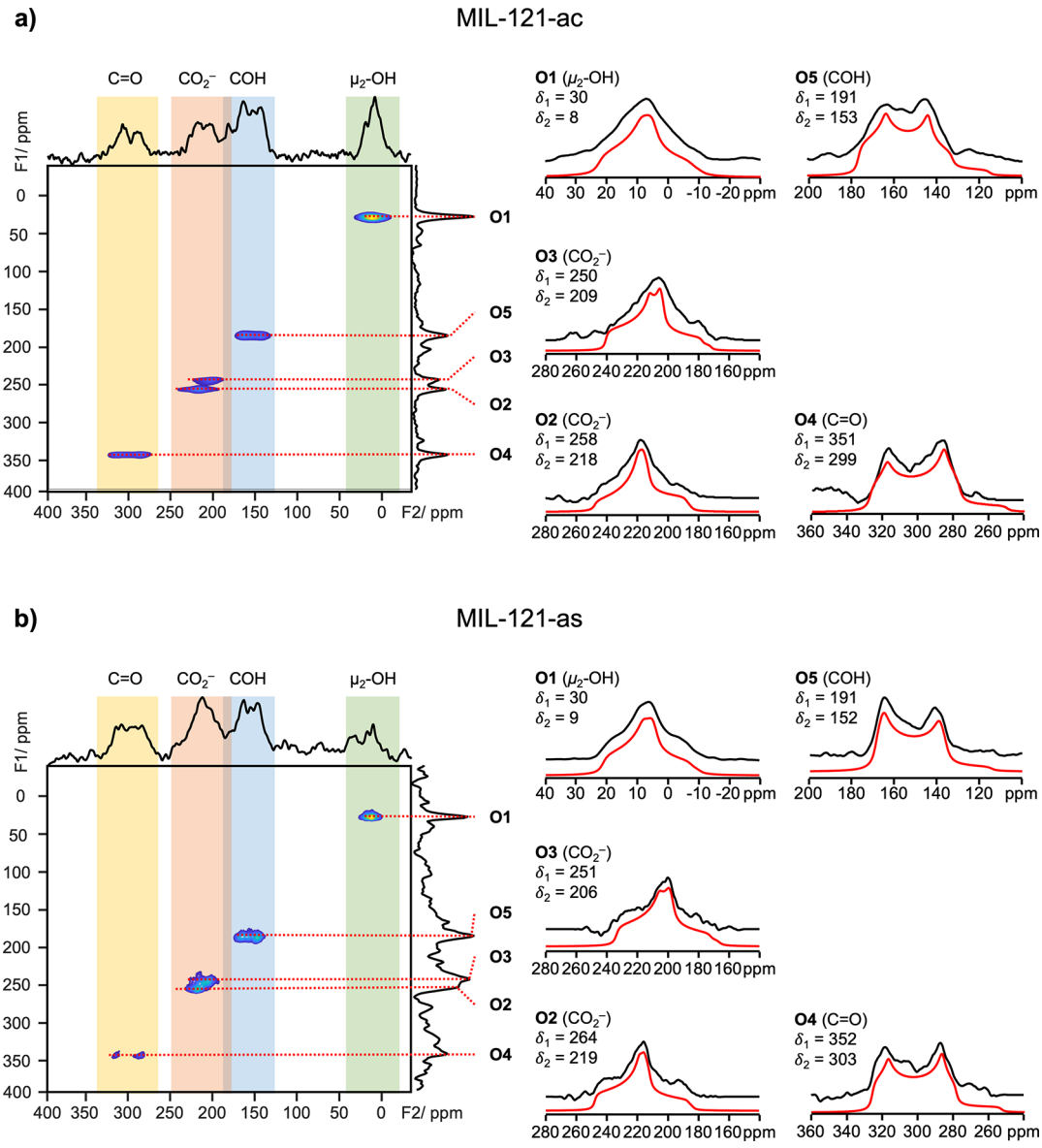

Figure 6. ^{17}O 2D 3QMAS NMR spectra of (a) MIL-121-ac and (b) MIL-121-as at 19.6 T with a spinning rate of 16 kHz. On the right, the experimental spectral slices for each O signal in the F2 dimension are shown in black with corresponding simulations of the experimental data shown below in red. δ_1 denotes the observed shift in the indirect (F1) direction, δ_2 is the spectral center of gravity along the direct (F2) dimension. These are not to be confused with the chemical shift tensor components δ_{XX}, δ_{YY}, and δ_{ZZ}.

are well-resolved in the 3QMAS spectrum and exhibit distinct chemical shift values of δ_{iso} = 235 and 243 ppm in MIL-121-as with similar values of δ_{iso} = 234 and 247 ppm in MIL-121-ac. A 3QMAS spectrum of MIL-121-as was also acquired at 35.2 T (Figure S4) but did not yield any additional insight. At this point, data external to NMR experiments is required in order to conclusively assign these two resonances to the O2 and O3 crystallographic sites.

Ab Initio Calculations. In order to guide the assignment of the O2 and O3 ^{17}O NMR resonances to crystallographic oxygen sites, gauge-including projector augmented wave (GIPAW) density functional theory (DFT) calculations[51−53] were performed and compared to experimental ^{17}O NMR results. The GIPAW or "plane-wave DFT" approach has proven to be very reliable for ^{17}O NMR spectral assignment in a variety of systems.[54,62−66] All experimental ^{17}O NMR parameters for the O2 and O3 sites in MIL-121-as and -ac are quite similar, particularly C_Q and η_Q (Table S8); δ_{iso} is the only way to distinguish between O2 and O3 since it varies beyond experimental measurement uncertainty. The calculated ^{17}O NMR parameters are listed in Tables S10−S13 and visualized as spectra in Figure 7. A summary of the calculation strategy and results follows with additional details provided in the Experimental Section and Supporting Information.

For calculations on MIL-121-as, the unit cell parameters and atomic positions from the reported MIL-121-as crystal structure[10] were used as a starting point. The uncoordinated pyromellitic acid guest molecules in the pores were removed to model MIL-121-ac. In both MOFs, insertion of any necessary hydrogen atoms was followed by geometry optimization of all atomic positions. ^{17}O NMR calculations in MIL-121-ac were performed using a unit cell containing four O1 (μ_2-OH), eight O2 (CO_2^-), eight O3 (CO_2^-), eight O4 (C═O), and eight O5 (COH) atoms, which produced four sets of calculated

https://doi.org/10.1021/acs.chemmater.3c00199
Chem. Mater. 2023, 35, 3555−3569

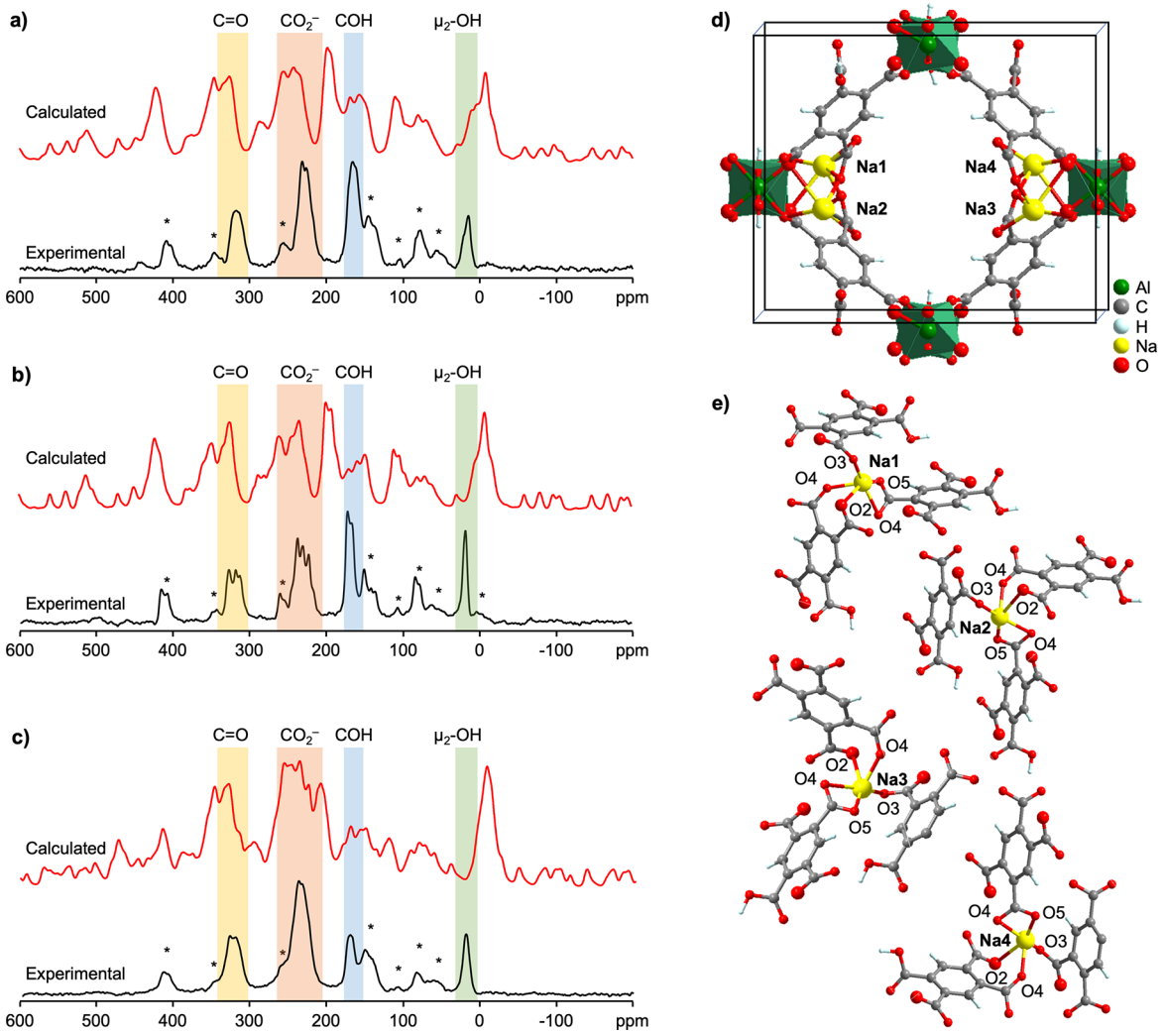

Figure 7. Experimental and calculated ^{17}O 1D MAS spectra of (a) MIL-121-as, (b) MIL-121-ac, and (c) Na@MIL-121 samples acquired at 35.2 T with a spinning rate of 18 kHz. The asterisks (*) in experimental spectra mark spinning sidebands. In the calculated spectra, an overestimation of CSA leads to spinning sidebands that are far more intense than those observed experimentally. (d) A single unit cell of the Na@MIL-121 MOF that was used for ab initio calculations at a 50% Na loading level is shown, as projected along the *c* axis. (e) The calculated local environments of the four sodium atoms in 50% Na loaded Na@MIL-121 are illustrated.

NMR parameters for O1 and eight sets of NMR parameters for each of O2, O3, O4, and O5. The presence of the μ_2-OH hydrogen atoms with an occupancy of 0.5 breaks the initial symmetry. For as-made MIL-121, calculations required a double unit cell along the *c* direction to properly encompass and model uncoordinated pyromellitic acid in the pore (Figure S6). In MIL-121-as, 8 sets of parameters were obtained for O1, 16 sets of parameters were obtained for O2, O3, O4, and O5, and 2 sets of parameters were calculated for each of O21−O28 on the unreacted BTEC guest molecule in the pores. The range in calculated parameters for any given unique O site was small in both systems. An average of calculated NMR parameters for each O site were then tabulated and compared to experimental values. The MIL-121 crystal structure indicates that the C═O distance in C═O4 is shorter than that of C═O5 in the linker carboxylic acid group, which places the acidic hydrogen on O5. This assignment was verified using DFT calculations; see Tables S10−S13 with hydrogen located on O4 and O5. The structure of MIL-121 using the O5 acidic proton position generally yielded calculated ^{17}O NMR results that were more accurate and consistent with experimental values for both phases, which strongly suggests that the reported XRD structure is correct. Going forward, only results obtained with hydrogen on O5 are discussed; calculated results using hydrogen bound to O4 can be found in Tables S12 and S13. Of note is that using hydrogen on O4 also yields the same calculated δ_{iso} trends that support our O2 and O3 assignments below.

Calculations produced δ_{iso} values in both MIL-121-as and -ac that were in good agreement with experimental results (Figure 7 and Table S14). There was a small overestimate in δ_{iso} for all oxygen environments except O1 (μ_2-OH), which was slightly underestimated. The accuracy of calculated versus experimental δ_{iso} values shows that these results can be used to assign the O2 and O3 signals. Although calculated δ_{iso} values do not exactly match experimental values, assignments of multiple ^{17}O signals in the same spectrum on the basis of their relative calculated δ_{iso} values is a valid approach.[54,62−67] The relative calculated δ_{iso} values between oxygen environments is in line with experimental observations for previously assigned sites. The calculated δ_{iso} trend for both MOF phases is O4 > O2 > O3 > O5 > O1, while the experimental trend is O4 >

https://doi.org/10.1021/acs.chemmater.3c00199
Chem. Mater. 2023, 35, 3555−3569

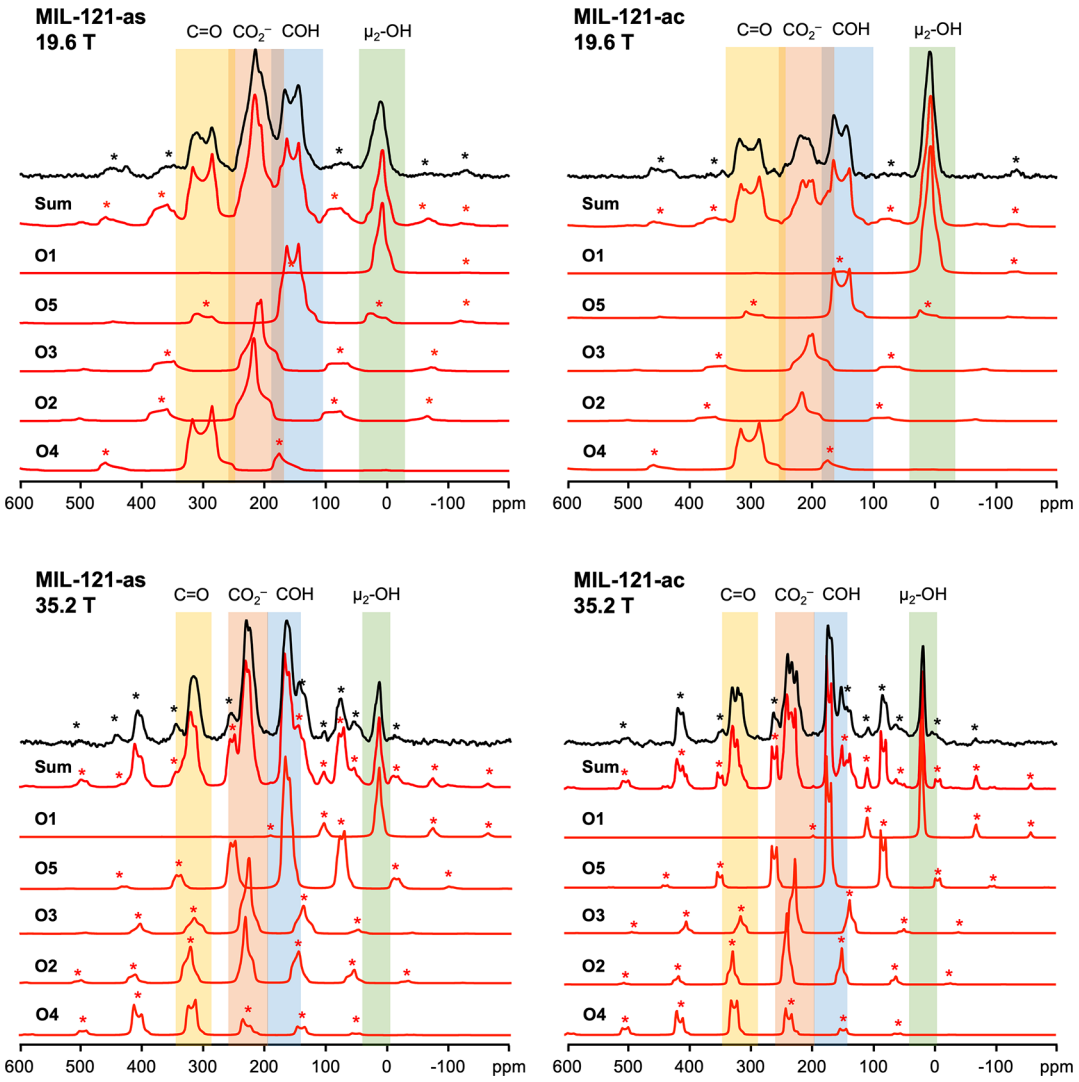

Figure 8. Experimental and simulated ^{17}O 1D MAS spectra of MIL-121-ac and MIL-121-as acquired at 19.6 T and 35.2 T with spinning rates of 16 and 18 kHz, respectively. The experimental spectra are shown in black with simulations in red. Spinning sidebands are denoted by an asterisk (*).

O2/O3 > O5 > O1, suggesting that, of the overlapping O2 and O3 ^{17}O NMR signals, the resonance of the larger δ_{iso} should correspond to O2. In both MOF phases, O2 was calculated to have a higher shift than O3. The O2 − O3 difference in calculated δ_{iso} values is 22 ppm in MIL-121-as and 26 ppm in MIL-121-ac. Experimentally, the difference in δ_{iso} between the two O2/O3 signals is smaller but still significant at 9 ppm in MIL-121-as and 13 ppm in MIL-121-ac. Based on the calculated chemical shifts for the overlapping O2/O3 ^{17}O NMR signals in both MIL-121-as and -ac, the resonance of the higher δ_{iso} is assigned to O2 and the signal of the lower δ_{iso} is assigned to O3. The calculated δ_{iso} values of O2 and O3 were ca. 25 and 12 ppm higher than experimental findings, respectively, in both MIL-121-ac and -as.

There are several other observations regarding the general accuracy of other calculated ^{17}O NMR parameters in these systems. The calculated ^{17}O C_Q values for each specific oxygen environment in MIL-121-as and -ac were all overestimated, which is consistent with recent reports regarding ^{17}O NMR calculations that involve MOFs.[27,28] This overestimation can be attributed to the effect of dynamics, which are not taken into account by this computational approach. The overestimation in C_Q is particularly noticeable for the O1 (μ_2-OH) site, which points into the MOF interior and can thus engage in hydrogen bonding with guests. The ^{17}O chemical shift of O1 is also underestimated by calculations. The dynamics in question are likely related to the rotation of the hydrogen atom within the −OH group where the hydrogen is subject to a fast reorientation in a cone-shaped space about the −OH bond through the whole cone region or within a discrete section of the cone. Within MIL-121-as containing guest H_2O, there are −OH flipping dynamics that may occur. Both types of hydrogen motion would increase the spherical symmetry about oxygen and thus reduce the experimentally observed $C_Q(^{17}O)$ values.

Aside from dynamics, the discrepancy between calculated and experimental C_Q(O1) and δ_{iso}(O1) values may also be caused by (i) inaccurate modeling of hydrogen bonding, (ii) the intrinsic disorder of guest H_2O and BTEC molecules in the system, and (iii) a poor estimate of the bond distance between O1 and one or more of its neighbors. The calculated η_Q values were in good agreement with experimental data for all sites except O4, which implies that there is slightly more rotational symmetry about O4 versus what is indicated from the crystal structure. Unfortunately, calculations of the Δ_{CS}, η_{CS}, and Euler angle parameters were not particularly accurate as seen from

https://doi.org/10.1021/acs.chemmater.3c00199
Chem. Mater. 2023, 35, 3555−3569

Table 1. Refined[a] ^{17}O EFG and CS Parameters of MIL-121-as and MIL-121-ac

sample	site	O type	integration (%)	δ_{iso} (ppm)	C_Q (MHz)	η_Q	Δ_{CS} (ppm)	η_{CS}	ϕ (°)	χ (°)	ψ (°)
MIL-121-as	O1	μ_2-OH	13(2)	23(2)	5.3(1)	0.80(5)	−120(10)	0.20(5)	180(10)	20(10)	0(10)
	O5	COH	34(2)	173(2)	6.6(1)	0.20(5)	160(10)	1.00(5)	110(10)	60(10)	100(10)
	O3	CO_2^-	21(2)	235(2)	6.6(1)	0.90(5)	200(10)	1.00(5)	30(10)	60(10)	0(10)
	O2	CO_2^-	20(2)	244(2)	6.6(1)	0.90(5)	210(10)	1.00(5)	30(10)	0(10)	0(10)
	O4	C═O	12(2)	328(2)	8.0(1)	0.20(5)	−200(10)	0.50(5)	30(10)	30(10)	0(10)
MIL-121-ac	O1	μ_2-OH	24(2)	22(2)	4.7(1)	0.80(5)	120(10)	1.00(5)	0(10)	30(10)	30(10)
	O5	COH	20(2)	177(2)	7.3(1)	0.15(5)	180(10)	0.00(5)	0(10)	0(10)	30(10)
	O3	CO_2^-	17(2)	235(2)	7.3(1)	0.80(5)	200(10)	1.00(5)	30(10)	60(10)	0(10)
	O2	CO_2^-	17(2)	248(2)	7.3(1)	0.90(5)	210(10)	1.00(5)	30(10)	0(10)	0(10)
	O4	C═O	22(2)	333(2)	8.0(1)	0.20(5)	−200(10)	1.00(5)	90(10)	60(10)	0(10)

[a]The refined parameters were obtained from the experimental simulations shown in Figure 8; see main text for a detailed description of the simulation refinement protocol.

the calculated spectra in Figure 7 including CSA effects and are not discussed in further detail. It must be noted that structural data in the literature for the MIL-121 system is sparse; the only available crystal structure describes MIL-121-as,[10] includes disordered guest H_2O and BTEC molecules, and lacks some hydrogen positions. Despite this challenge, the protocol of using DFT geometry optimizations followed by GIPAW calculation of ^{17}O NMR parameters in MIL-121-ac works very well for the assignment of ^{17}O resonances to oxygen sites based on relative chemical shifts. The calculation strategy also yields reasonably accurate estimates of δ_{iso}, η_Q, and C_Q for MIL-121-ac; this approach clearly holds great promise for applications to many other MOF systems with crystal structures of various quality levels.

Refinement of ^{17}O NMR Parameters. Generally, to accurately simulate the solid-state NMR spectra of a nucleus subject to the quadrupolar and CS interactions such as ^{17}O, datasets from at least two considerably different magnetic fields are desired, owing to the opposing EFG and CS magnetic field dependencies. Information gleaned from 3QMAS experiments is also useful, but even with this additional insight, it remains challenging to reconcile a set of ^{17}O NMR parameters that successfully fit all experimental spectra at both fields due to the overwhelming number of variables. In this instance, a comprehensive simulation of a 1D ^{17}O MAS spectrum with five inequivalent oxygen sites while considering both the EFG and CS interactions is nearly impossible without preliminary steps as this would require the independent refinement of 40 parameters. Our simulation protocol was designed to reduce simulation complications without sacrificing accuracy. The 1D ^{17}O MAS spectrum at 19.6 T was first simulated using the C_Q, η_Q, and δ_{iso} values obtained from 3QMAS experiments at 19.6 T (Table S9) as initial inputs. Only C_Q, η_Q, and δ_{iso} values were refined due to the stronger EFG and weaker CS manifestation at this field, and they were then used as starting points for simulating 1D MAS spectra at 35.2 T to extract the CS parameters. The initial CS values for simulations, including the reduced anisotropy (Δ_{CS}) and the chemical shift asymmetry parameter (η_{CS}), were taken from reported values for oxalic acid (Table S9)[68] and varied to fit the spinning sideband pattern at 35.2 T. The three Euler angles ϕ, χ, and ψ were introduced and fit at this stage. All parameters were then slightly adjusted to fit the ^{17}O MAS NMR spectra at 19.6 and 35.2 T (Figure S5). The average of values obtained from both fields was used to simulate the ^{17}O MAS NMR spectra of MIL-121-as and -ac (Figure 8) and reported as the final refined EFG and CS parameters (Table 1). There are no discernable ^{17}O signals from the unreacted ligands in MIL-121-as with hypothesized reasoning detailed in footnote a of Table S8.

^{17}O NMR of Metal-Exchanged MIL-121 Samples. With the oxygen sites of MIL-121 characterized by ^{17}O NMR and assigned to crystallographic sites, it is possible to monitor changes in the local environment of framework oxygen atoms upon the introduction of guest species. This route should provide a deeper understanding of guest locations and any associated structural effects on the MOF. Loading guest metal ions into MOFs offers the opportunity to introduce new properties or tune existing ones, particularly regarding applications in gas adsorption and catalysis.[4,6,7,17,69] The MIL-121 MOF is an excellent target for ^{17}O NMR since prior work has shown that guest metals exchange for hydrogen atoms on the uncoordinated carboxylic acid groups of the linkers, resulting in a CO_2^- linker group bound to the guest metal.[17] ^{17}O NMR studies of metal−carbonyl interactions in organic and biological molecules[22] have shown that this technique provides direct information on structural changes and host−guest interactions. While the metal loading has been shown to reduce the Brunauer−Emmett−Teller (BET) surface area of MIL-121 when N_2 was used as the probe gas, CO_2 and H_2 adsorption were substantially increased;[17] this illustrates the potential applications of these materials and also indicates that the MOF pores remain intact after metal loading.

MIL-121 was loaded with several different metals with the resulting materials termed M@MIL-121 (M = Na^+, Ca^{2+}, Ag^+, and In^{3+}). These metals were chosen to build on a previous study[17] that examined the impact of MIL-121 metal doping from the guest metal perspective. The degree of metal ion exchange for carboxylic acid hydrogen was measured by ICP-MS (Table S15), which indicated that the metal exchange was 42.0% for Na, 5.0% for Ca, 30.0% for Ag, and 6.5% for In. Further details regarding metal exchange calculations are in Table S15 footnote a. The ^{17}O 1D MAS spectra of the most extensively metal-exchanged materials, namely Na@MIL-121 and Ag@MIL-121, exhibit the largest deviations in appearance versus MIL-121-ac (Figure 9) with the ^{17}O 1D MAS spectra of other metal-loaded MIL-121 samples collected in Figure S7.

A clear change in the relative intensity between the COH and CO_2^- ^{17}O NMR signals is apparent after loading Na^+ and Ag^+ (Table 2). In MIL-121-ac, prior to guest loading, the ^{17}O COH resonance is stronger than that of CO_2^-, and the COH:CO_2^- spectral intensity ratio is 1(0.23):0.86(0.07) (i.e., 21(5):18(1.4) in Table 2); this is within experimental uncertainty to the 1:1 ratio indicated from the crystal structure. Upon Na^+ and Ag^+ exchange, the relative intensity of the ^{17}O

https://doi.org/10.1021/acs.chemmater.3c00199
Chem. Mater. 2023, 35, 3555−3569

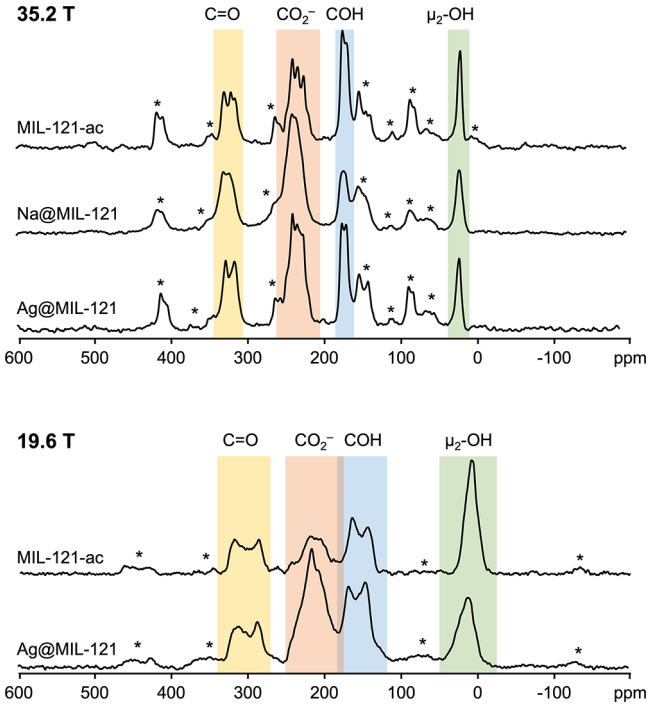

Figure 9. Experimental ^{17}O 1D MAS spectra of MIL-121-ac and Na^+/Ag^+@MIL-121 acquired at different magnetic fields with spinning rates of 16 kHz (19.6 T) and 18 kHz (35.2 T). The spinning sidebands are denoted by an asterisk (*).

Table 2. Intensity Differences in ^{17}O NMR Signals upon Metal Exchange

O site	O type	before metal exchange	after Na^+ exchange	after Ag^+ exchange
O1	μ_2-OH	46(5)	27(5)	23(5)
O5	COH	21(5)	21(5)	29(5)
O3	CO_2^-	9(1)	21(5)	23(5)
O2	CO_2^-	9(1)	21(5)	17(5)
O4	C═O	14(5)	11(5)	8(1)

COH resonance decreases significantly versus the CO_2^- NMR signal, and the COH:CO_2^- ratio becomes ca. 1:2, which indicates that a significant portion of the COOH groups are now CO_2^- groups. Removal of the acidic proton in a COOH group by acid−base neutralization or ion exchange (e.g., with a guest metal ion) leads to the formation of a CO_2^- group whose chemical shift lies between that of C═O and COH[56,57,70] and is very similar to that of linker CO_2^- groups coordinated to framework Al,[40] resulting in an increased ^{17}O signal intensity in that spectral region. The ^{17}O NMR COH:CO_2^- intensity data indicates that the Na^+ exchange level in Na@MIL-121 is ca. 50%, which agrees with the value of 42% from ICP-MS. The ^{17}O NMR COH:CO_2 intensity data suggests a Ag^+ metal exchange level in Ag@MIL-121 of ca. 25%, which is near the 30% from ICP-MS. It should be made clear that ^{17}O NMR is not more analytically accurate than ICP-MS; however, ^{17}O NMR may be used in a semi-quantitative manner to estimate the degree of guest metal exchange.

There is a significant decrease in the ^{17}O NMR signal intensity corresponding to μ_2-OH groups after metal exchange in the Na@MIL-121 and Ag@MIL-121 systems. The ^{17}O MAS NMR spectra were acquired using a spin-echo pulse sequence in which the relative ^{17}O signal intensity may be influenced by the transverse magnetization relaxation time (T_2) of the oxygen nucleus; large reductions in T_2 for ^{17}O in the μ_2-OH groups after the exchange explains the observed reduction in the ^{17}O NMR signal intensity. There was no significant change observed in the ^{17}O NMR COH and CO_2^- spectral region for Ca@MIL-121 and In@MIL-121 with measured intensity ratios found to be the same as in MIL-121-ac. ICP-MS experiments indicated that metal loading levels were ca. 5% for both Ca@MIL-121 and In@MIL-121; the small amounts of ion-exchange in these two samples are likely too low to produce significant effects in the corresponding ^{17}O NMR spectra, and thus they are not discussed in detail any further.

Additional qualitative information can be gleaned from the ^{17}O MAS NMR spectral lineshapes of Na@MIL-121 and Ag@MIL-121. When Ag^+ is loaded, there is no significant loss of resolution, and there are noticeable lineshape changes in the CO_2^-, C═O, and COH regions, indicating that Ag^+ binding affects the local environment of all these oxygen species on the free carboxyl groups of the MIL-121 linkers. The overall spectral resolution is generally preserved, which suggests that the framework structure remains intact and short-range order exists about nearly every unique oxygen site. These ^{17}O NMR findings are consistent with prior ^{1}H and ^{13}C NMR studies along with X-ray absorption spectroscopy (XAS) experiments on Ag@MIL-121,[17] in which Ag^+ was found to reside in an acetate-like environment and was proposed to bind with O4 and O5 of the COOH group after substituting for the acidic H atom.

The introduction of Na^+ guests to MIL-121 strongly impacts the ^{17}O MAS NMR spectrum. There is a loss of fine resolution throughout with all distinct ^{17}O signal groups broadened and featureless. Previous ^{23}Na NMR results (Figure S8) indicated that Na^+ ions are randomly distributed around carboxylate groups in this system,[17] which would give rise to a distribution of oxygen environments and loss of ^{17}O NMR lineshape features. The combined ^{17}O and ^{23}Na NMR data indicates that Na^+ ions are distributed in a disorganized fashion throughout the pores of Na@MIL-121 and not strictly in locations immediately proximate to the free carboxyl groups.

^{17}O 3QMAS experiments (Figures S9 and S10) were carried out on the metal-exchanged materials to further investigate the location and binding of guest metal cations. The 3QMAS spectra of Ag@MIL-121 and In@MIL-121 are very similar to that of MIL-121-ac with only two signals observed in the CO_2^- region and no new signals apparent. In contrast, the F2 slices of the Na@MIL-121 ^{17}O 3QMAS spectrum at each oxygen signal are rather featureless, indicating that local disorder exists about each oxygen site. The broadened peaks in each characteristic ^{17}O δ_{iso} region for Na@MIL-121 confirms a distribution of ^{17}O environments that are slightly different from each of the O1−O5 environments, supporting a distribution of O sites residing in a disordered local environment; unfortunately, discrete signals within these distributions could not be individually resolved with sufficient resolution and intensity to perform comprehensive simulations. The ^{17}O NMR parameters for O1−O5 obtained from 3QMAS experiments on Ag@MIL-121 and Na@MIL-121 (Table S16) do not differ significantly from those of MIL-121-ac.

Ab Initio Calculations of ^{17}O NMR Parameters in Na@MIL-121. To further investigate the incorporation of guest metal ions, ab initio calculations of the sodium-loaded MIL-121 sample were performed using the MIL-121-ac structure as

https://doi.org/10.1021/acs.chemmater.3c00199
Chem. Mater. 2023, 35, 3555−3569

a starting point. The sodium atoms were added to the vicinity of the free carboxylate groups after the hydrogen atoms were removed, and all atomic positions were then optimized. Recall that, upon Na^+ loading, an additional ^{17}O NMR signal intensity arises in the CO_2^- region, while the intensity of the COH region decreases due to the exchange of Na^+ for the acidic carboxyl hydrogen atom. As with previous calculations, the unit cell contained four O1 (μ_2-OH), eight O2 (CO_2^-), eight O3 (CO_2^-), eight O4 (C═O), and eight O5 (COH) atoms, which produced four sets of calculated NMR parameters for O1 and eight sets of NMR parameters for each of O2, O3, O4, and O5. In order to model the 50% exchange of carboxyl hydrogen atoms with Na^+ ions indicated from ^{17}O MAS NMR experiments, hydrogen atoms were allowed to remain bound to four O5 sites, while hydrogen was replaced by Na^+ ions at the four remaining O5 centers. This is equivalent to a 50% exchange. After optimization, the spectral parameters were calculated and are summarized in Table S17. A lower Na^+ exchange amount of 37% was also explored with five protons and three sodium cations attached to O5 (Table S18), which will not be discussed.

Calculations using a 50% Na loading level indicate that there should be four crystallographic inequivalent Na^+ cations present in the unit cell of Na@MIL-121 (Figure 7d). While there are four unique Na^+ sites, a closer examination of the local Na environment in Figure 7e illustrates how all four Na^+ sites reside in similar chemical environments. Each Na^+ interacts with the O4 and O5 oxygen atoms on the free carboxylate group as well as with the O2 and O3 oxygens bound to the aluminum centers. The distribution of similar local Na environments explains the rather broad, featureless ^{23}Na NMR signal that was previously reported in this system (Figure S8).[17]

The presence of multiple similar Na^+ sites proximate to O2, O3, O4, and O5 indicated from ^{23}Na NMR and ab initio calculations agrees well with the distribution of ^{17}O local environments at those oxygen sites indicated from the ^{17}O 3QMAS experiments. At a 50% Na loading level, calculations situate half of the O2, O3, O4, and O5 sites near Na^+, which gives rise to even more disorder about the O2−O5 sites that serves to further broaden ^{17}O NMR signals and reduce the spectral resolution in a specific region. This is in good agreement with the loss of fine details in the C═O, CO_2^-, and COH regions of the Na@MIL-121 ^{17}O NMR spectrum when compared to that of empty MIL-121-ac in Figure 9 and with the distribution of oxygen environments indicated by the broadened peaks in the ^{17}O 3QMAS spectrum of Na@MIL-121 in Figure S10. A comparison of MIL-121-ac and Na@MIL-121 calculated and experimental ^{17}O NMR parameters (Table S19) reveals small changes in δ_{iso} for O1, O2, and O3 before and after the introduction of Na^+ guests, which would contribute to the experimentally observed loss of ^{17}O spectral resolution. The O4 and O5 signals are also of significant interest. In the Na^+ loading procedure, the free COOH group in MIL-121 is first deprotonated to a CO_2^- group and then becomes a C═ONa moiety. The C═ONa signal from O4 (formerly C═O) was calculated to have a δ_{iso} of 276 ppm. Given the overestimation of ca. 20 ppm in calculated δ_{iso} values for MIL-121-ac, this O4 calculation in Na@MIL-121 is interpreted to mean that a new ^{17}O NMR signal on the high-frequency side of the CO_2^- spectral region at ca. 255 ppm would be expected after Na^+ introduction. The calculated position of this O4 signal in Na@MIL-121 would make it difficult to identify in a spectral region already occupied by the existing O2 and O3 CO_2^- signals and influenced by local disorder. The C═ONa signal from O5 is calculated to resonate at 392 ppm, which is not evident in ^{17}O NMR MAS spectra. However, again assuming that the consistent overestimation persists in ^{17}O δ_{iso} calculations, this signal would likely be at least 20 ppm lower, which would place the O5 signal in the existing C═O spectral region with multiple other oxygen NMR signals also affected by local disorder. Given those circumstances, the C═ONa signal from O5 cannot be conclusively identified. While the ^{17}O NMR spectrum of Na-bound ^{17}O nuclei could not be completely resolved experimentally, ab initio calculations have provided insight explaining the loss of spectral resolution at the O2, O3, O4, and O5 signals in Na@MIL-121 while also rationalizing the intensity changes between these spectral regions.

CONCLUSIONS

This work illustrates how ^{17}O NMR at high magnetic fields can resolve all unique ^{17}O signals originating from multiple forms of a complex MOF, including activated and metal-loaded derivatives, and provides molecular-level information on the local oxygen environment. ^{17}O NMR is a sensitive probe for investigating both coarse and fine structural features in MOFs. 1D MAS ^{17}O NMR spectra at 19.6 and 35.2 T have been correlated to bound linkers, bridging hydroxyl moieties, and free carboxylic acid groups within the as-made, activated, and metal-loaded variants of MIL-121. A protocol employing ^{17}O MAS, $^{17}O/^1H$ D-HMQC, $^{17}O\{^1H\}$ REDOR, and 3QMAS NMR experiments alongside detailed ab initio calculations achieved unambiguous spectral assignment of ^{17}O resonances to chemically and crystallographically unique sites in MOFs. A complete set of ^{17}O NMR parameters for each of the five chemically/crystallographically non-equivalent sites in the MIL-121 crystal structure was obtained using ^{17}O 3QMAS experiments at 19.6 T to extract quadrupolar parameters and ^{17}O MAS NMR experiments at 35.2 T to quantify CS parameters; this data was then refined against spectra from both fields to unify the simulations, yielding the final NMR parameters. Building on this data, the incorporation of metal guests within MIL-121 could then be examined via ^{17}O NMR, which was shown to provide a reasonable estimate of guest loading while shedding light on metal-binding sites and areas of local disorder triggered by guest metal loading within the MOF. In particular, it was evident that Na^+ guests are located at multiple sites within MIL-121 and contribute to the local disorder about oxygen sites.

High-field ^{17}O NMR is a powerful tool for the characterization of MOFs and the investigation of processes relevant to practical applications of these materials, including activation and guest loading. Oxygen is ubiquitous in MOF linkers, functional groups, and guests, often playing an integral role in structural stability and function; ^{17}O NMR characterization of local structures is critical given the fundamental importance of this element. ^{17}O NMR shows great promise for understanding PSM processes and pathways to unlocking additional MOF properties in addition to pinpointing the structural origins of unique attributes. Multinuclear NMR approaches including ^{17}O offer tremendous promise for detailed characterization of diverse MOFs and will undoubtedly be a powerful tool for probing these materials in future years.

https://doi.org/10.1021/acs.chemmater.3c00199
Chem. Mater. 2023, 35, 3555−3569

■ ASSOCIATED CONTENT

Supporting Information

The Supporting Information is available free of charge at https://pubs.acs.org/doi/10.1021/acs.chemmater.3c00199.

Powder X-ray patterns, TGA profiles, additional experimental and simulated ^{17}O MAS and 3QMAS data of pristine and metal-loaded MIL-121, ^{17}O enrichment details, experimental NMR details, and tabulated experimental and calculated ^{17}O NMR parameters (PDF)

■ AUTHOR INFORMATION

Corresponding Author

Yining Huang − *Department of Chemistry, The University of Western Ontario, London, Ontario, Canada N6A 5B7;* orcid.org/0000-0001-9265-5896; Email: yhuang@uwo.ca

Authors

Vinicius Martins − *Department of Chemistry, The University of Western Ontario, London, Ontario, Canada N6A 5B7*

Bryan E.G. Lucier − *Department of Chemistry, The University of Western Ontario, London, Ontario, Canada N6A 5B7;* orcid.org/0000-0002-9682-4324

Kuizhi Chen − *National High Magnetic Field Laboratory (NHMFL), Tallahassee, Florida 32310, United States;* orcid.org/0000-0002-9853-7070

Ivan Hung − *National High Magnetic Field Laboratory (NHMFL), Tallahassee, Florida 32310, United States;* orcid.org/0000-0001-8916-739X

Zhehong Gan − *National High Magnetic Field Laboratory (NHMFL), Tallahassee, Florida 32310, United States;* orcid.org/0000-0002-9855-5113

Christel Gervais − *Sorbonne Universieť, CNRS, UMR 7574, Laboratoire de Chimie de la Matière Condensée de Paris, LCMCP, F-75005 Paris, France*

Christian Bonhomme − *Sorbonne Universieť, CNRS, UMR 7574, Laboratoire de Chimie de la Matière Condensée de Paris, LCMCP, F-75005 Paris, France;* orcid.org/0000-0003-0802-6961

Heng-Yong Nie − *Surface Science Western, The University of Western Ontario, London, Ontario, Canada N6G 0J3;* orcid.org/0000-0002-8287-5171

Wanli Zhang − *Department of Chemistry, The University of Western Ontario, London, Ontario, Canada N6A 5B7*

Complete contact information is available at: https://pubs.acs.org/10.1021/acs.chemmater.3c00199

Author Contributions

#V.M. and B.E.G.L. contributed equally to this work.

Notes

The authors declare no competing financial interest.

■ ACKNOWLEDGMENTS

A portion of this work was performed at the National High Magnetic Field Laboratory (NHMFL, USA), which is supported by NSF DMR-1644779 and the State of Florida. The SCH magnet and NMR instrumentation was supported by the NSF (nos. DMR-1039938 and DMR-0603042) and NIH (no. BTRR 1P41 GM122698). The authors would like to thank Dr. Victor Terskikh (Metrology, National Research Council Canada) for preliminary ^{17}O NMR experiments on MIL-121 at a magnetic field of 21.1 T. Y.H. thanks the Natural Science and Engineering Research Council (NSERC) of Canada for a Discovery Grant. DFT calculations were performed using HPC resources from GENCI-IDRIS (grant no. 097535).

■ REFERENCES

(1) Yuan, S.; Feng, L.; Wang, K.; Pang, J.; Bosch, M.; Lollar, C.; Sun, Y.; Qin, J.; Yang, X.; Zhang, P.; Wang, Q.; Zou, L.; Zhang, Y.; Zhang, L.; Fang, Y.; Li, J.; Zhou, H.-C. Stable Metal−Organic Frameworks: Design, Synthesis, and Applications. *Adv. Mater.* **2018**, *30*, No. e1704303.

(2) Ryu, U.; Jee, S.; Rao, P. C.; Shin, J.; Ko, C.; Yoon, M.; Park, K. S.; Choi, K. M. Recent Advances in Process Engineering and Upcoming Applications of Metal−Organic Frameworks. *Coord. Chem. Rev.* **2021**, *426*, No. 213544.

(3) Safaei, M.; Foroughi, M. M.; Ebrahimpoor, N.; Jahani, S.; Omidi, A.; Khatami, M. A Review on Metal-Organic Frameworks: Synthesis and Applications. *TrAC, Trends Anal. Chem.* **2019**, *118*, 401−425.

(4) Mandal, S.; Natarajan, S.; Mani, P.; Pankajakshan, A. Post-Synthetic Modification of Metal−Organic Frameworks Toward Applications. *Adv. Funct. Mater.* **2021**, *31*, 2006291.

(5) Kalaj, M.; Cohen, S. M. Postsynthetic Modification: An Enabling Technology for the Advancement of Metal−Organic Frameworks. *ACS Cent. Sci.* **2020**, *6*, 1046−1057.

(6) Islamoglu, T.; Goswami, S.; Li, Z.; Howarth, A. J.; Farha, O. K.; Hupp, J. T. Postsynthetic Tuning of Metal-Organic Frameworks for Targeted Applications. *Acc. Chem. Res.* **2017**, *50*, 805−813.

(7) Yin, Z.; Wan, S.; Yang, J.; Kurmoo, M.; Zeng, M. H. Recent Advances in Post-Synthetic Modification of Metal−Organic Frameworks: New Types and Tandem Reactions. *Coord. Chem. Rev.* **2019**, *378*, 500−512.

(8) Chen, S.; Song, Z.; Lyu, J.; Guo, Y.; Lucier, B. E. G.; Luo, W.; Workentin, M. S.; Sun, X.; Huang, Y. Anhydride Post-Synthetic Modification in a Hierarchical Metal-Organic Framework. *J. Am. Chem. Soc.* **2020**, *142*, 4419−4428.

(9) Bhadra, B. N.; Ahmed, I.; Lee, H. J.; Jhung, S. H. Metal-Organic Frameworks Bearing Free Carboxylic Acids: Preparation, Modification, and Applications. *Coord. Chem. Rev.* **2022**, *450*, No. 214237.

(10) Volkringer, C.; Loiseau, T.; Guillou, N.; Ferey, G.; Haouas, M.; Taulelle, F.; Elkaim, E.; Stock, N. High-Throughput Aided Synthesis of the Porous Metal− Organic Framework-Type Aluminum Pyromellitate, MIL-121, with Extra Carboxylic Acid Functionalization. *Inorg. Chem.* **2010**, *49*, 9852−9862.

(11) Serre, C.; Millange, F.; Thouvenot, C.; Noguès, M.; Marsolier, G.; Louër, D.; Férey, G. Very Large Breathing Effect in the First Nanoporous Chromium(III)-Based Solids: MIL-53 or $Cr^{III}(OH)\{O_2C\text{-}C_6H_4\text{-}CO_2\}\{HO_2C\text{-}C_6H_4\text{-}CO_2H\}_x\cdot H_2O_y$. *J. Am. Chem. Soc.* **2002**, *124*, 13519−13526.

(12) Loiseau, T.; Serre, C.; Huguenard, C.; Fink, G.; Taulelle, F.; Henry, M.; Bataille, T.; Férey, G. A Rationale for the Large Breathing of the Porous Aluminum Terephthalate (MIL-53) Upon Hydration. *Chem. − Eur. J.* **2004**, *10*, 1373−1382.

(13) Chen, S.; Mukherjee, S.; Lucier, B. E. G.; Guo, Y.; Wong, Y. T. A.; Terskikh, V. V.; Zaworotko, M. J.; Huang, Y. Cleaving Carboxyls: Understanding Thermally Triggered Hierarchical Pores in the Metal-Organic Framework MIL-121. *J. Am. Chem. Soc.* **2019**, *141*, 14257−14271.

(14) Ji, C.; Wu, D.; Lu, J.; Shan, C.; Ren, Y.; Li, T.; Lv, L.; Pan, B.; Zhang, W. Temperature Regulated Adsorption and Desorption of Heavy Metals to A-MIL-121: Mechanisms and the Role of Exchangeable Protons. *Water Res.* **2021**, *189*, No. 116599.

(15) Zettl, R.; Lunghammer, S.; Gadermaier, B.; Boulaoued, A.; Johansson, P.; Wilkening, H. M. R.; Hanzu, I. High Li^+ and Na^+ Conductivity in New Hybrid Solid Electrolytes Based on the Porous MIL-121 Metal Organic Framework. *Adv. Energy Mater.* **2021**, *11*, 2003542.

(16) Ou, R.; Zhang, H.; Wei, J.; Kim, S.; Wan, L.; Nguyen, N. S.; Hu, Y.; Zhang, X.; Simon, G. P.; Wang, H. Thermoresponsive Amphoteric Metal−Organic Frameworks for Efficient and Reversible Adsorption of Multiple Salts from Water. *Adv. Mater.* **2018**, *30*, 1802767.
(17) Chen, S.; Lucier, B. E. G.; Luo, W.; Xie, X.; Feng, K.; Chan, H.; Terskikh, V. V.; Sun, X.; Sham, T. K.; Workentin, M. S.; Huang, Y. Loading Across the Periodic Table: Introducing 14 Different Metal Ions to Enhance Metal-Organic Framework Performance. *ACS Appl. Mater. Interfaces* **2018**, *10*, 30296−30305.
(18) Loiseau, T.; Volkringer, C.; Haouas, M.; Taulelle, F.; Férey, G. Crystal Chemistry of Aluminium Carboxylates: From Molecular Species Towards Porous Infinite Three-Dimensional Networks. *C. R. Chim.* **2015**, *18*, 1350−1369.
(19) Sutrisno, A.; Huang, Y. Solid-State NMR: A Powerful Tool for Characterization of Metal-Organic Frameworks. *Solid State Nucl. Magn. Reson.* **2013**, *49*, 1−11.
(20) Lucier, B. E. G.; Chen, S.; Huang, Y. Characterization of Metal-Organic Frameworks: Unlocking the Potential of Solid-State NMR. *Acc. Chem. Res.* **2018**, *51*, 319−330.
(21) Li, S.; Lafon, O.; Wang, W.; Wang, Q.; Wang, X.; Li, Y.; Xu, J.; Deng, F. Recent Advances of Solid-State NMR Spectroscopy for Microporous Materials. *Adv. Mater.* **2020**, *32*, 2002879.
(22) Palmer, J.; Wu, G. Recent Developments in ^{17}O NMR Studies of Organic and Biological Molecules in the Solid State. *Annu. Rep. NMR Spectrosc.* **2021**, *103*, 1−46.
(23) Ashbrook, S. E.; Davis, Z. H.; Morris, R. E.; Rice, C. M. ^{17}O NMR Spectroscopy of Crystalline Microporous Materials. *Chem. Sci.* **2021**, *12*, 5016−5036.
(24) Carnevale, D.; Mouchaham, G.; Wang, S.; Baudin, M.; Serre, C.; Bodenhausen, G.; Abergel, D. Natural Abundance Oxygen-17 Solid-State NMR of Metal Organic Frameworks Enhanced by Dynamic Nuclear Polarization. *Phys. Chem. Chem. Phys.* **2021**, *23*, 2245−2251.
(25) He, P.; Xu, J.; Terskikh, V. V.; Sutrisno, A.; Nie, H. Y.; Huang, Y. Identification of Nonequivalent Framework Oxygen Species in Metal-Organic Frameworks by ^{17}O Solid-State NMR. *J. Phys. Chem. C* **2013**, *117*, 16953−16960.
(26) Rice, C. M.; Davis, Z. H.; McKay, D.; Bignami, G. P. M.; Chitac, R. G.; Dawson, D. M.; Morris, R. E.; Ashbrook, S. E. Following the Unusual Breathing Behaviour of ^{17}O-Enriched Mixed-Metal (Al,Ga)-MIL-53 Using NMR Crystallography. *Phys. Chem. Chem. Phys.* **2020**, *22*, 14514−14526.
(27) Bignami, G. P. M.; Davis, Z. H.; Dawson, D. M.; Morris, S. A.; Russell, S. E.; McKay, D.; Parke, R. E.; Iuga, D.; Morris, R. E.; Ashbrook, S. E. Cost-Effective ^{17}O Enrichment and NMR Spectroscopy of Mixed-Metal Terephthalate Metal−Organic Frameworks. *Chem. Sci.* **2018**, *9*, 850−859.
(28) Leroy, C.; Métro, T.-X.; Hung, I.; Gan, Z.; Gervais, C.; Laurencin, D. From Operando Raman Mechanochemistry to "NMR Crystallography:" Understanding the Structures and Interconversion of Zn-Terephthalate Networks Using Selective ^{17}O-Labeling. *Chem. Mater.* **2022**, *34*, 2292−2312.
(29) Martins, V.; Xu, J.; Wang, X.; Chen, K.; Hung, I.; Gan, Z.; Gervais, C.; Bonhomme, C.; Jiang, S.; Zheng, A.; Lucier, B. E. G.; Huang, Y. Higher Magnetic Fields, Finer MOF Structural Information: ^{17}O Solid-State NMR at 35.2 T. *J. Am. Chem. Soc.* **2020**, *142*, 14877−14889.
(30) Martins, V.; Xu, J.; Hung, I.; Gan, Z.; Gervais, C.; Bonhomme, C.; Huang, Y. ^{17}O Solid-State NMR at Ultrahigh Magnetic Field of 35.2 T: Resolution of Inequivalent Oxygen Sites in Different Phases of MOF MIL-53(Al). *Magn. Reson. Chem.* **2021**, *59*, 940−950.
(31) Demong, D. E.; Ng, I.; Miller, M. W.; Stamford, A. W. A Novel Method for the Preparation of 4-Arylimidazolones. *Org. Lett.* **2013**, *15*, 2830−2833.
(32) U.S. EPA. *Method 200.8: Determination of Trace Elements in Waters and Wastes by Inductively Coupled Plasma-Mass Spectrometry*; 1994, U.S. EPA: Revision 5.4. Cincinnati, OH, USA.
(33) Gan, Z.; Hung, I.; Wang, X.; Paulino, J.; Wu, G.; Litvak, I. M.; Gor'kov, P. L.; Brey, W. W.; Lendi, P.; Schiano, J. L.; Bird, M. D.; Dixon, I. R.; Toth, J.; Boebinger, G. S.; Cross, T. A. NMR Spectroscopy up to 35.2 T Using a Series-Connected Hybrid Magnet. *J. Magn. Reson.* **2017**, *284*, 125−136.
(34) Harris, R. K.; Becker, E. D.; de Menezes, S. M. C.; Goodfellow, R.; Granger, P. NMR Nomenclature. Nuclear Spin Properties and Conventions for Chemical Shifts (IUPAC Recommendations 2001). *Pure Appl. Chem.* **2001**, *73*, 1795−1818.
(35) Gullion, T.; Schaefer, J. Rotational-Echo Double-Resonance NMR. *J. Magn. Reson.* **1989**, *81*, 196−200.
(36) Gullion, T. Introduction to Rotational-Echo, Double-Resonance NMR. *Concepts Magn. Reson.* **1998**, *10*, 277−289.
(37) Gan, Z.; Amoureux, J. P.; Trébosc, J. Proton-Detected ^{14}N MAS NMR Using Homonuclear Decoupled Rotary Resonance. *Chem. Phys. Lett.* **2007**, *435*, 163−169.
(38) Cavadini, S.; Abraham, A.; Bodenhausen, G. Proton-Detected Nitrogen-14 NMR by Recoupling of Heteronuclear Dipolar Interactions Using Symmetry-Based Sequences. *Chem. Phys. Lett.* **2007**, *445*, 1−5.
(39) Brinkmann, A.; Kentgens, A. P. M. Proton-Selective ^{17}O−H Distance Measurements in Fast Magic-Angle-Spinning Solid-State NMR Spectroscopy for the Determination of Hydrogen Bond Lengths. *J. Am. Chem. Soc.* **2006**, *128*, 14758−14759.
(40) Massiot, D.; Touzo, B.; Trumeau, D.; Coutures, J. P.; Virlet, J.; Florian, P.; Grandinetti, P. J. Two-Dimensional Magic-Angle Spinning Isotropic Reconstruction Sequences for Quadrupolar Nuclei. *Solid State Nucl. Magn. Reson.* **1996**, *6*, 73−83.
(41) Massiot, D. Sensitivity and Lineshape Improvements of MQ-MAS by Rotor-Synchronized Data Acquisition. *J. Magn. Reson., Ser. A* **1996**, *122*, 240−244.
(42) Frydman, L.; Harwood, J. S. Isotropic Spectra of Half-Integer Quadrupolar Spins from Bidimensional Magic-Angle Spinning NMR. *J. Am. Chem. Soc.* **1995**, *117*, 5367−5368.
(43) Hung, I.; Trébosc, J.; Hoatson, G. L.; Vold, R. L.; Amoureux, J. P.; Gan, Z. Q-Shear Transformation for MQMAS and STMAS NMR Spectra. *J. Magn. Reson.* **2009**, *201*, 81−86.
(44) Massiot, D.; Fayon, F.; Capron, M.; King, I.; Le Calvé, S.; Alonso, B.; Durand, J. O.; Bujoli, B.; Gan, Z.; Hoatson, G. Modelling One- and Two-Dimensional Solid-State NMR Spectra. *Magn. Reson. Chem.* **2002**, *40*, 70−76.
(45) Pyykkö, P. Year-2017 Nuclear Quadrupole Moments. *Mol. Phys.* **2018**, *116*, 1328−1338.
(46) Kresse, G.; Hafner, J. *Ab Initio* Molecular-Dynamics Simulation of the Liquid-Metal−Amorphous-Semiconductor Transition in Germanium. *Phys. Rev. B* **1994**, *49*, 14251.
(47) Giannozzi, P.; Baroni, S.; Bonini, N.; Calandra, M.; Car, R.; Cavazzoni, C.; Ceresoli, D.; Chiarotti, G. L.; Cococcioni, M.; Dabo, I.; Corso, A. D.; de Gironcoli, S.; Fabris, S.; Fratesi, G.; Gebauer, R.; Gerstmann, U.; Gougoussis, C.; Kokalj, A.; Lazzeri, M.; Martin-Samos, L.; Marzari, N.; Mauri, F.; Mazzarello, R.; Paolini, S.; Pasquarello, A.; Paulatto, L.; Sbraccia, C.; Scandolo, S.; Sclauzero, G.; Seitsonen, A. P.; Smogunov, A.; Umari, P.; Wentzcovitch, R. M. QUANTUM ESPRESSO: A Modular and Open-Source Software Project for Quantum of Materials. *J. Condens. Matter Phys.* **2009**, *21*, 395502.
(48) Perdew, J. P.; Burke, K.; Ernzerhof, M. Generalized Gradient Approximation Made Simple. *Phys. Rev. Lett.* **1996**, *77*, 3865.
(49) Troullier, N.; Martins, J. L. Efficient Pseudopotentials for Plane-Wave Calculations. *Phys. Rev. B* **1991**, *43*, 1993.
(50) Kleinman, L.; Bylander, D. M. Efficacious Form for Model Pseudopotentials. *Phys. Rev. Lett.* **1982**, *48*, 1425.
(51) Pickard, C. J.; Mauri, F. All-Electron Magnetic Response with Pseudopotentials: NMR Chemical Shifts. *Phys. Rev. B* **2001**, *63*, No. 245101.
(52) Charpentier, T. The PAW/GIPAW Approach for Computing NMR Parameters: A New Dimension Added to NMR Study of Solids. *Solid State Nucl. Magn. Reson.* **2011**, *40*, 1−20.

https://doi.org/10.1021/acs.chemmater.3c00199
Chem. Mater. 2023, 35, 3555−3569

(53) Bonhomme, C.; Gervais, C.; Babonneau, F.; Coelho, C.; Pourpoint, F.; Azais, T.; Ashbrook, S. E.; Griffin, J. M.; Yates, J. R.; Mauri, F. First-Principles Calculation of NMR Parameters Using the Gauge Including Projector Augmented Wave Method: A Chemist's Point of View. *Chem. Rev.* **2012**, *112*, 5733−5779.
(54) Métro, T.-X.; Gervais, C.; Martinez, A.; Bonhomme, C.; Laurencin, D. Unleashing the Potential of ^{17}O NMR Spectroscopy Using Mechanochemistry. *Angew. Chem., Int. Ed.* **2017**, *129*, 6907−6911.
(55) Wu, G. ^{17}O NMR Studies of Organic and Biological Molecules in Aqueous Solution and in the Solid State. *Prog. Nucl. Magn. Reson. Spectrosc.* **2019**, *114*−*115*, 135−191.
(56) Hagaman, E. W.; Chen, B.; Jiao, J.; Parsons, W. Solid-State ^{17}O NMR Study of Benzoic Acid Adsorption on Metal Oxide Surfaces. *Solid State Nucl. Magn. Reson.* **2012**, *41*, 60−67.
(57) Rees, G. J.; Day, S. P.; Lari, A.; Howes, A. P.; Iuga, D.; Pitak, M. B.; Coles, S. J.; Threlfall, T. L.; Light, M. E.; Smith, M. E.; Quigley, D.; Wallis, J. D.; Hanna, J. V. A Multinuclear Solid State NMR, Density Functional Theory and X-Ray Diffraction Study of Hydrogen Bonding in Group I Hydrogen Dibenzoates. *CrystEngComm* **2013**, *15*, 8823−8839.
(58) Schaefer, J. Development of REDOR Rotational-Echo Double-Resonance NMR. *J. Magn. Reson.* **2011**, *213*, 421−422.
(59) Gullion, T. Measurement of Dipolar Interactions between Spin-1/2 and Quadrupolar Nuclei by Rotational-Echo, Adiabatic-Passage, Double-Resonance NMR. *Chem. Phys. Lett.* **1995**, *246*, 325−330.
(60) Medek, A.; Harwood, J. S.; Frydman, L. Multiple-Quantum Magic-Angle Spinning NMR: A New Method for the Study of Quadrupolar Nuclei in Solids. *J. Am. Chem. Soc.* **1995**, *117*, 12779−12787.
(61) Amoureux, J. P.; Fernandez, C.; Steuernagel, S. Z-Filtering in MQMAS NMR. *J. Magn. Reson., Ser. A* **1996**, *123*, 116−118.
(62) Romao, C. P.; Perras, F. A.; Werner-Zwanziger, U.; Lussier, J. A.; Miller, K. J.; Calahoo, C. M.; Zwanziger, J. W.; Bieringer, M.; Marinkovic, B. A.; Bryce, D. L.; White, M. A. Zero Thermal Expansion in $ZrMgMo_3O_{12}$: NMR Crystallography Reveals Origins of Thermoelastic Properties. *Chem. Mater.* **2015**, *27*, 2633−2646.
(63) Kong, X.; Terskikh, V. V.; Khade, R. L.; Yang, L.; Rorick, A.; Zhang, Y.; He, P.; Huang, Y.; Wu, G. Solid-State ^{17}O NMR Spectroscopy of Paramagnetic Coordination Compounds. *Angew. Chem., Int. Ed.* **2015**, *54*, 4753−4757.
(64) Wang, M.; Wu, X. P.; Zheng, S.; Zhao, L.; Li, L.; Shen, L.; Gao, Y.; Xue, N.; Guo, X.; Huang, W.; Gan, Z.; Blanc, F.; Yu, Z.; Ke, X.; Ding, W.; Gong, X. Q.; Grey, C. P.; Peng, L. Identification of Different Oxygen Species in Oxide Nanostructures with ^{17}O Solid-State NMR Spectroscopy. *Sci. Adv.* **2015**, *1*, No. e1400133.
(65) Pavón, E.; Osuna, F. J.; Alba, M. D.; Delevoye, L. Natural Abundance ^{17}O MAS NMR and DFT Simulations: New Insights into the Atomic Structure of Designed Micas. *Solid State Nucl. Magn. Reson.* **2019**, *100*, 45−51.
(66) Sutrisno, A.; Lucier, B. E. G.; Zhang, L.; Ding, L.; Chu, Y.; Zheng, A.; Huang, Y. Inspecting the Structure and Formation of Molecular Sieve SAPO-34 via ^{17}O Solid-State NMR Spectroscopy. *J. Phys. Chem. C* **2018**, *122*, 7260−7277.
(67) Li, Y.; Wu, X.-P.; Jiang, N.; Lin, M.; Shen, L.; Sun, H.; Wang, Y.; Wang, M.; Ke, X.; Yu, Z.; Gao, F.; Dong, L.; Guo, X.; Hou, W.; Ding, W.; Gong, X.-Q.; Grey, C. P.; Peng, L. Distinguishing Faceted Oxide Nanocrystals with ^{17}O Solid-State NMR Spectroscopy. *Nat. Commun.* **2017**, *8*, 581.
(68) Zhang, Q.; Chekmenev, E. Y.; Wittebort, R. J. ^{17}O Quadrupole Coupling and Chemical Shielding Tensors in an H-Bonded Carboxyl Group: α-Oxalic Acid. *J. Am. Chem. Soc.* **2003**, *125*, 9140−9146.
(69) Ji, G.; Gao, X.; Zheng, T.; Guan, W.; Liu, H.; Liu, Z. Postsynthetic Metalation Metal−Organic Framework as a Fluorescent Probe for the Ultrasensitive and Reversible Detection of PO_4^{3-} Ions. *Inorg. Chem.* **2018**, *57*, 10525−10532.
(70) Wong, A.; Pike, K. J.; Jenkins, R.; Clarkson, G. J.; Anupõld, T.; Howes, A. P.; Crout, D. H. G.; Samoson, A.; Dupree, R.; Smith, M. E. Experimental and Theoretical ^{17}O NMR Study of the Influence of Hydrogen-Bonding on CO and O−H Oxygens in Carboxylic Solids. *J. Phys. Chem. A* **2006**, *110*, 1824−1835.

https://doi.org/10.1021/acs.chemmater.3c00199
Chem. Mater. 2023, 35, 3555−3569